FATIGUE STRENGTH OF DETERIORATED AND PREVIOUSLY STRESSED STEEL HIGHWAY BRIDGES

FHWA-RIDOT-RTD-02-4
JULY 2002

George Tsiatas
Everett McEwen
Arun Shukla
Shane Palmquist

University of Rhode Island

Sponsored By Rhode Island Department of Transportation

Rhode Island
Department of Transportation

RESEARCH AND
TECHNOLOGY
DEVELOPMENT

Technical Report Documentation Page

1. Report No.	2. Government Accession No.	3. Recipient's Catalog No.
FHWA-RI-RTD-02-4		

4. Title and Subtitle	5. Report Date
Fatigue Strength of Deteriorated and Previously Stressed Steel Highway Bridges	June 2002
	6. Performing Organization Code

7. Author(s)	8. Performing Organization Report No.
George Tsiatas, Everett McEwen, Arun Shukla, Shane Palmquist	URI-CVE-ST02-4

9. Performing Organization Name and Address	10. Work Unit No. (TRAIS)
Civil Engineering Department University of Rhode Island Kingston, RI 02881	11. Contract or Grant No. SPR-2 (26) 2226

12. Sponsoring Agency Name and Address	13. Type of Report and Period Covered
Rhode Island Department of Transportation Two Capitol Hill Providence, RI	Final Report
	14. Sponsoring Agency Code

15. Supplementary Notes

16. Abstract

This study provides a comparison of four procedures to determine the fatigue life of steel bridges, namely the AASHTO *Guide Specifications*, BAR7, the Lehigh method, and fracture mechanics (LEFM). Results demonstrate that fatigue predictions made using the AASHTO *Guide Specifications* and LEFM are more accurate than the other two methods. Several details are examined using AASHTO guidelines and linear fracture mechanics principles where the time required for an initial flaw to propagate to a critical depth is calculated. It is found that fatigue lives of actual bridges as determined using fracture mechanics far exceed the remaining safe fatigue life predictions made with current AASHTO guide specifications. For the case of redundant bridges, an adjustment factor is introduced which, at various probability levels, can produce closer estimates of bridge fatigue lives between the AASHTO specifications and fracture mechanics.

17. Key Word	18. Distribution Statement
Bridges Fatigue Condition Assessment	No Restrictions

19. Security Classif. (of this report)	20. Security Classif. (of this page)	21. No. of Pages	22. Price
Unclassified	Unclassified	129	

Disclaimer

This report was sponsored by the Rhode Island Department of Transportation. The contents of the report reflect the views of the authors who are responsible for the facts and accuracy of the data presented herein. The contents do not necessarily reflect the official views or policies of the Rhode Island Department of Transportation or the US Department of Transportation's Federal Highway Administration. This report does not constitute a standard, specification, or regulation.

TABLE OF CONTENTS

LIST OF SYMBOLS

SYMBOL	MEANING, METHOD
a	present age of the bridge, AASHTO *Guide Specifications*
a	crack length, LEFM
a_{cr}	critical crack length, LEFM
a_i	initial crack length, LEFM
A	fatigue factor depending on the AASHTO fatigue category of the detail which relates the stress range to the number of accumulated cycles, BAR7
ADT	average daily traffic
$ADTT$	average daily truck traffic
b	half the flange width of the girder, LEFM
c	half the length of the crack oriented perpendicular to the live load stress range, LEFM
c_f	fatigue factor relating the stress range to the number of accumulated cycles
C	stress cycles per truck passage, AASHTO *Guide Specifications*
C	average crack growth metal constant, LEFM
D, D_{-1}, D_{+1}	span factor corresponding to span lengths, L, L_{-1}, and L_{+1}, respectively, AASHTO *Guide Specifications*
DF	distribution factor
DF_e	distribution factor for an exterior member, AASHTO *Guide Specifications*
DF_i	distribution factor for an interior member, AASHTO *Guide Specifications*
DF_1	distribution factor for one traffic lane, BAR7

f	safe or mean fatigue life factor, AASHTO *Guide Specifications*
f_{sr}	fatigue stress, BAR7
$(f_{sr})_e$	effective fatigue stress range, BAR7
$(f_{sr})_D$	design fatigue stress range, BAR7
F_e	elliptical crack shape correction factor, LEFM
F_g	stress gradient correction factor, LEFM
F_s	free surface correction factor, LEFM
F_{sr}	allowable stress range, AASHTO *Specifications*
F_w	finite width or thickness correction factor, LEFM
F_L	fraction of trucks in outer lane, AASHTO *Guide Specifications*
F_{S1}	procedure factor for stress range used to determine the reliability factor, R_S, AASHTO *Guide Specifications*
F_{S2}	procedure factor for gross weight of fatigue truck used to determine the reliability factor, R_S, AASHTO *Guide Specifications*
F_{S3}	procedure factor for lateral distribution factor used to determine the reliability factor, R_S, AASHTO *Guide Specifications*
F_T	fraction of trucks, AASHTO *Guide Specifications*
g	traffic (truck) growth rates, AASHTO *Guide Specifications*
GF_1	past growth factor, BAR7
GF_2	future growth factor, BAR7
I	inertia
I_f	impact factor, BAR7
I_T	total inertia of all applicable sections

K	detail constant relating its susceptibility to fatigue damage, AASHTO *Guide Specifications*
K	stress intensity factor, LEFM
K_c	fracture toughness of the metal, LEFM
K_{max}	stress intensity factor corresponding to the on set of rapid crack growth, LEFM
K_{th}	fatigue threshold, LEFM
K_{Ic}	critical stress intensity factor for plane strain condition, LEFM
L, L_{-1}, L_{+1}	span lengths, L_{-1} and L_{+1} correspond to the table in section 2.6.1, AASHTO *Guide Specifications*
m	metal constant, LEFM
M	moment
M	accumulated number of cycles, BAR7
M_{live}	maximum algebraic difference between the positive live load moment and the negative live load moment including the impact factor
n	present age of bridge, BAR7
n_i	accumulated number of cycles at stress range, S_{ri}
n_f	future year for which *ADTT* is estimated, BAR7
n_1	previous year which *ADTT* is known, BAR7
n_2	recent year which *ADTT* is known, BAR7
n_3	difference between n_1 and n_2, BAR7
n_4	difference between n_f and n_2, BAR7
N	accumulated number of fatigue cycles
N	design fatigue life in cycles, BAR7
N	total fatigue life in cycles, LEFM
N_i	constant amplitude cycles to failure at stress range, S_{ri}

N_T	accumulated number of cycles, Lehigh
PTF	Pennsylvania traffic factor used in calculating the effective fatigue stress range, $(f_{sr})_e$, used in the fatigue life equation, BAR7
R	remaining fatigue life in years, BAR7
R_f	redundancy factor, AASHTO *Guide Specifications*
$R_{m\text{-}s}$	ratio of total mean life to total safe life
R_S	reliability factor, AASHTO *Guide Specifications*
R_{S0}	basic redundant or nonredundant reliability factor, AASHTO *Guide Specifications*
S	girder spacing, AASHTO *Guide Specifications*
S_c	compressive dead load stress, AASHTO *Guide Specifications*
S_r	nominal stress range, AASHTO *Guide Specifications*
S_r	maximum stress range due to live load, LEFM
S_{re}	effective fatigue stress range, Lehigh
S_{ri}	stress range
S_{ri}	stress range, Lehigh
S_{rmax}	maximum stress range, Lehigh
S_t	tension portion of stress range, AASHTO *Guide Specifications*
S_{FL}	limiting stress range for infinite fatigue life, AASHTO *Guide Specifications*
S_R	stress range resulting from applied live load
t	member thickness, LEFM
t_c	cover plate thickness, LEFM
t_f	flange thickness, LEFM

t_w	web thickness, LEFM
T_a	estimated lifetime average daily traffic, *ADT*, volume in the outer lane, AASHTO *Guide Specifications*
w	member width, LEFM
y	distance from the neutral axis to the location of the detail
Y_f	remaining fatigue life in years, AASHTO *Guide Specifications*
Z	weld leg size, LEFM
$^{da}/_{dN}$	crack growth rate per cycle of loading, LEFM
α	method of structural analysis factor used to determine the effective fatigue stress range, $(f_{sr})_e$, BAR7
β	safety index, NCHRP 299
γ	summation factor for effective fatigue stress range, $(f_{sr})_e$, BAR7
γ	reliability factor, NCHRP 299
γ_i	percentage frequency of occurrence for stress range, S_{ri}, Lehigh
ΔK	stress intensity factor range, LEFM
$\Delta\sigma$	live load stress range, LEFM
θ	angle for an elliptical crack, LEFM
σ	axial stress
σ_{peak}	peak stress range, LEFM
σ_{ys}	plane strain yield strength, LEFM
$\Phi(-\beta)$	nominal failure probability, NCHRP 299

LIST OF TABLES

LIST OF FIGURES

1.0 INTRODUCTION

Fatigue is an important issue in the service life of any existing steel bridge. Bridge failures including: the Mianus River Bridge in Connecticut, the Point Pleasant Bridge in Ohio, the County Highway 28 Bridge in Illinois, the Quinnipiac River Bridge in Connecticut, and numerous others, demonstrate this.

Fatigue is the process of cumulative damage of a material subjected to net cyclic tensile stress. It begins with microcracks at the material's surface and/or interior. These microcracks as well as larger ones called macro cracks propagate with each stress cycle. Stress cycles are caused by trucks traveling across the bridge. Four and five axle semi-trailers cause nearly all fatigue damage (Moses, Schilling, and Raju 1987). As a result of these semi-trailers, details of steel bridges with long service lives have accumulated millions of cycles of stress.

Details are fatigue prone for one or more of the following reasons: abrupt change in geometry, change in homogeneity, poor weld quality, or a location along the span where the nominal stress range is maximized. All of these conditions contribute to highly localized tensile stress at the detail. This may be significantly above the yield strength of the material while the global stress surrounding the detail is well below the yield strength. At the detail, these stress concentrations promote microcrack growth. This often leads to macro crack growth and eventual fracture. The previously mentioned bridges are examples of crack growth which led to fracture.

Soon after the occurrence of these bridge failures, the phenomenon of fatigue was investigated. A new section in the AASHTO *Specifications* addressed fatigue considerations for the design of fatigue prone details. For design, the section combined an artificially high stress range with an artificially low number of cycles to produce a reasonable design. This procedure is not representative of actual conditions where the nominal stress range is well below yielding and the number of cycles is high. In addition, these considerations are for design purposes, not for fatigue evaluations of existing bridges. As a result of these inadequacies, other methods of fatigue evaluation emerged.

Four of these are discussed herein. They are: the AASHTO *Guide Specifications*, BAR7, the Lehigh method, and Linear Elastic Fracture Mechanics (LEFM.

The AASHTO *Guide Specifications* represent a probabilistic limit-state approach offering a consistent and reliable system for fatigue evaluation. One of the major components is the use of a special fatigue truck modeling truck traffic which brings the calculated stress range to more realistic levels than earlier AASHTO *Specifications*. Two levels of fatigue performance can be estimated, namely the remaining mean fatigue life and the remaining safe fatigue life. The first corresponds to a 50 percent probability of exceedance whereas the second corresponds to a 97.7 percent probability for details with redundant members that the actual fatigue life will exceed the predicted value. For details with nonredundant members, this probability is 99.9 percent.

The AASHTO *Guide Specifications* was published in November 1987. The authors are F. Moses, C. G. Schilling, and K. S. Raju. Written with the intent of being incorporated in the AASHTO *Specifications*, the 1990 edition of the AASHTO *Guide Specifications* includes these modifications.

The Pennsylvania Department of Transportation created a computer program used exclusively to aid civil engineers in rating and fatigue evaluations of existing steel bridges. This program named BAR7 represents a deterministic approach to fatigue evaluation. Knowing the local truck traffic volume and growth, the total fatigue life in cycles can be determined as well as the number of accumulated stress cycles. Using an empirical equation, the remaining fatigue life in years can also be determined. BAR7, version 7.1, was published in 1991. The authors are H. M. Lathia and J. A. Breon.

At the ATLSS Engineering Research Center of Lehigh University, J. W. Fisher, B. T. Yen, and D. Wang proposed a deterministic procedure for approximating the fatigue damage in existing steel bridges. In the Lehigh method, the number the accumulated cycles is evaluated and plotted with the corresponding stress range. Also plotted is the *SN* curve for that particular AASHTO fatigue category. The relative position of the two is a measure of the remaining fatigue life.

LEFM has also been used to evaluate fatigue life for details of existing steel bridges (Fisher 1984). Estimates of fatigue life are based on macro crack propagation only. Crack initiation, microcrack growth, and crack growth beyond the critical crack size are not considered.

In practice, the following methods are used: the AASHTO *Guide Specifications*, BAR7, and the Lehigh method. LEFM is typically used in practice only after a member has already failed. Reliable data can then be obtained by an analysis of the crack surface. As a result, the predicted fatigue life is more accurate when failure has already occurred or data about the crack is available.

Other methods not discussed herein include: the rainflow counting method for fatigue analysis, a method proposed by Hahin et. al. (1993), and modal methods. In the rainflow counting method which is based on Miner's law, mean and amplitude values based on each loading are

identified to ensure that the appropriate amount of damage is properly counted (Hertzberg 1989). The method proposed by Hahin et. al. (1993) modifies Miner's law by a safety factor. Modal methods generally monitor changes in stiffness and mode shapes which can then be related to fatigue damage or other types of damage such as corrosion.

Only the AASHTO *Guide Specifications*, BAR7, the Lehigh method, and LEFM are discussed since these methods are commonly used in civil practice. These methods are summarized and outlined in Chapter 2. Two examples from actual bridges in Rhode Island are also included in this chapter as well as a comparison of all methods. In Chapter 3, three more examples are examined using the AASHTO *Guide Specifications* and LEFM. Chapter 4 discusses the results obtained using the AASHTO *Guide Specifications* and LEFM. In Chapter 5, the AASHTO *Guide Specifications* is calibrated to have a closer agreement with LEFM predictions. Chapter 6 discusses testing and monitoring fatigue prone details. A brief overview and conclusion is presented in Chapter 7.

2.0 CURRENT METHODS OF FATIGUE LIFE PREDICTION

2.1 Overview

Four methods of fatigue life prediction for steel girder or truss type bridges are discussed and outlined in this chapter. They are: the AASHTO *Guide Specifications*, BAR7, the Lehigh method, and LEFM. It is important to remember that fatigue life predictions represent the shortest time to fracture that may reasonably be expected. They are not precise measures of actual fatigue life. The purpose of these methods is to develop a reliable, consistent system of categorizing existing bridges for maintenance or replacement decisions. They also determine the need to perform nondestructive testing (Zuraski 1993).

Prior to using these methods, the detail is identified and the AASHTO fatigue category is determined. A list of details and their corresponding fatigue category is listed in the AASHTO *Specifications*, section 10.3 and in the Manual of Steel Construction (LRFD), section K3 of the Appendix. The categories are A, B, B', C, D, E, E', and F. The fatigue strength is highest for category A details and subsequently decreases for the remaining categories. Category F details which correspond to shear on the throat of a fillet weld rarely govern for fatigue, so this category is ignored.

2.2 AASHTO Guide Specifications

The AASHTO *Guide Specifications* approach has several limitations. The method is applicable for steel girder bridges with short to medium spans, not applicable to long span, cable-stayed, concrete, or prestressed concrete bridges. I-shaped, box-shaped, and truss elements may be evaluated. Members may be redundant or nonredundant. Only primary stresses are considered. The

contributions of secondary bending due to partial end fixity or member distortions are not addressed. This procedure is applicable to virgin, uncracked and unrepaired members except in the case of a retrofit of a welded cover plate end with bolt splices. Corrosion effects are not considered as well.

Determining the maximum range of live load stress at the detail is of extreme importance when evaluating the fatigue life. In the AASHTO *Guide Specifications*, this is called the nominal stress range. This may be found from: stress histograms, weigh-in-motion measurements near the site, fatigue-loading indicator (FLI) measurements, or finite element models.

FLI is a portable, battery-powered device that monitors random variable amplitude stress range at a detail. After performing the necessary calculations, it stores the equivalent constant amplitude fatigue loading (Chase 1995). This loading is then converted to the nominal stress range. This device is still being developed.

Often times sophisticated techniques of determining the stress range are not available due to time and money constraints, so the following simple equation is used,

$$\sigma = \frac{M \cdot y}{I} \qquad (2.1)$$

This states that the flexural stress, σ, in a homogenous, isotropic material may be calculated as the product of the moment, *M*, at the desired location and the distance, *y*, from the neutral axis of the section to the location of the detail. This is then divided by the moment of inertia, *I*, of the section. This equation is an expression for the normal stress at a detail. It is the stress range, not the normal stress, that is important when evaluating fatigue potential. This range results from the algebraic difference between the positive live load moment and the negative live load moment.

The moment is determined using the fatigue truck, Fig. 2.1. This truck is based on actual truck traffic spectrum from 30 sites nationwide and more than 27,000 observed trucks (Moses, Snyder, and Likins 1985).

A number of factors are applied to the above equation. They include: a distribution factor, an impact factor, a composite or noncomposite deck factor, and a truck bunching factor. These factors reflect recent research and can be easily modified to represent future trends and research.

The lateral distribution factor is applied to longitudinal bending members. This factor is applied to determine the portion of the maximum live load moment range carried by the specified member. The impact factor accounts for the condition of the pavement. Composite and noncomposite decks behave differently, so there is a factor which accounts for this. The last factor is used if bunching of trucks occurs such as a traffic signal on or near the bridge, or a steep hill when the bridge is on a two lane highway.

Fatigue life analysis of structural members, which are made of mild steel, is typically based on the power law expression for constant amplitude, high cycle fatigue,

$$N = \frac{c_f}{S_R^3} \tag{2.2}$$

c_f is a factor relating the stress range, S_R, to the accumulated number of fatigue cycles, N. This is consistent with Miner's law.

Normally, fatigue life is reported in terms of cycles. To convert from cycles to years, the following modification to c_f is required,

$$c_f = \frac{K \times 10^6}{T_a \cdot C} \tag{2.4}$$

Including two reliability factors f and R_S and replacing N with Y_f, the total fatigue life in years is,

$$Y_f = \frac{f \cdot K \times 10^6}{T_a \cdot C \cdot (R_S \cdot S_r)^3} \tag{2.3}$$

All of variables will be identified in the procedure below. Two types of fatigue calculations can be determined using this equation. They are the safe fatigue life and the mean fatigue life. The safe fatigue life corresponds to a probability of 97.7 percent for redundant members and 99.9 percent for non-redundant members that the actual fatigue life will exceed this. The mean fatigue life is the most likely probabilistic estimate of actual fatigue life given this methodology and the manner in which the parameters are determined. There is a 50 percent chance of exceeding the mean fatigue life. By subtracting the current age of a bridge from Eq. 2.3, its remaining safe or mean fatigue life can be found. The safe fatigue life is more conservative than the mean fatigue life. As a result, this is the value most frequently used for fatigue evaluations.

The following is an outline of the fatigue evaluation method as presented in the AASHTO *Guide Specifications*. As an additional note, modifications can be made to the procedure below to obtain more accurate values if the remaining safe fatigue life is inadequate. These modifications generally require more work to calculate and are infrequently used in practice. See appendix C of NCHRP 299. All references, unless otherwise noted, refer to the AASHTO Guide Specifications.

1. Obtain the limiting stress range for infinite fatigue life, S_{FL}, from section 3.3 in the AASHTO *Guide Specifications*. The S_{FL} value is similar to multiplying 0.367 by the allowable stress

range, F_{sr}, from the AASHTO *Specifications* table 10.3.1A with redundant load path structures for over 2,000,000 cycles.

2. Calculate the nominal stress range, S_r, at the detail,

$$S_r = \frac{(M_{live} \cdot DF) \cdot y}{I} \qquad (2.5)$$

M_{live} equals the maximum algebraic difference between the positive live load moment and the negative live load moment multiplied by the impact factor. For the moment calculation, use the fatigue truck as shown in figure 2.2A of the report. The dimensions and loads of this truck are as shown,

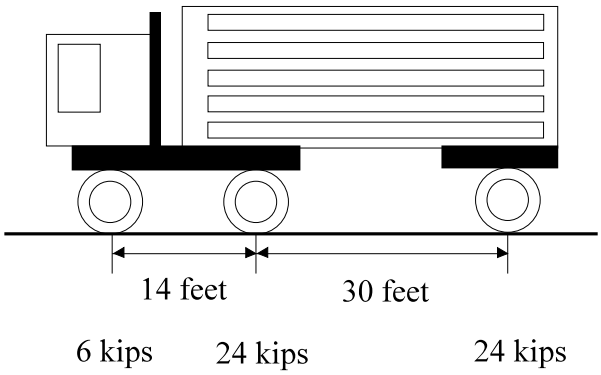

Fig. 2.1 Fatigue Truck, AASHTO *Guide Specifications*

The gross weight of the fatigue truck should be increased by a minimum of 10 percent to account for impact of smooth surfaces. If conditions are present such as poor expansion joints or rough pavement surfaces, the impact factor may be increased up to a maximum of 30 percent. See section 2.4. *DF* is the distribution factor in accordance with section 2.6. *y* is the distance from the neutral axis of the section to the location of the detail. The last term

is the moment of inertia of the section. For composite and noncomposite deck factors, see section 2.7. The gross weight of the fatigue truck may also be increased up to 15 percent if bunching of trucks occurs as discussed earlier.

3. Calculate the reliability factor, R_S,

$$R_S = R_{S0} \cdot F_{S1} \cdot F_{S2} \cdot F_{S3} \tag{2.6}$$

R_{S0} is the basic reliability factor. It equals 1.35 for redundant members and 1.75 for nonredundant members. F_{S1}, F_{S2}, and F_{S3} are procedure factors which account for the stress range, gross weight of fatigue truck, and lateral distribution, respectively. For the remaining mean fatigue life, R_S is 1.0.

4. Infinite life if, $R_S \cdot S_r < S_{FL}$ or $2 \cdot R_S \cdot S_t < S_c$

S_t equals the tension portion of the stress range, from section 2. S_c is the compressive dead load stress.

5. Calculate the remaining safe fatigue life or the remaining mean fatigue life in years, Y_f,

$$Y_f = \frac{f \cdot K \times 10^6}{T_a \cdot C \cdot (R_S \cdot S_r)^3} - a \tag{2.7}$$

K is a detail constant from section 3.3 relating its susceptibility to fatigue damage. It depends on the fatigue category of the detail. T_a is the estimated lifetime *ADTT* volume in the outer lane, see section 3.5. C is the number of stress cycles per truck passage from section 3.4. a is the present age of the bridge. Finally, f is the safe or mean fatigue life factor. This equals 1.0 for calculating the remaining safe fatigue life and 2.0 for calculating the remaining mean fatigue life.

2.3 BAR7

BAR7 is capable of performing fatigue evaluations on steel girder and truss type bridges of short to medium spans. Members may be redundant or non-redundant.

In BAR7, the maximum range in live load stress is called the design fatigue stress range. This may be found from the various procedures as mentioned in the previous section. It also may be calculated from the same simple equation,

$$\sigma = \frac{M \cdot y}{I} \tag{2.1}$$

The moment is determined using the HS20 truck. Factors are applied to the above equation. They include a distribution factor and an impact factor. The AASHTO *Specifications* lateral distribution factor is the maximum fraction of the axle load that is carried by the longitudinal member under investigation (Moses and Nyman 1984). It is based on all lanes loaded simultaneously. In addition, consideration is given to the worst possible longitudinal location of the truck with respect to the maximum moment. The impact factor accounts for dynamic, vibratory, and impact effects.

Fatigue life analysis is also based on the same equation which is consistent with Miner's law,

$$N = \frac{c_f}{S_R^3} \tag{2.8}$$

In BAR7, this equation appears as,

$$N = \frac{A}{(f_{sr})_e^3} \tag{2.9}$$

Knowing the past growth factor, GF_1, the age of the bridge, n, and the $ADTT$ for two separate years,

the accumulated number of cycles, M, can be calculated. This is determined using a uniform series compound factor,

$$\frac{(1 + GF_1)^n - 1}{GF_1}$$

From this, the accumulated number of the cycles is,

$$M = 365 \frac{days}{year} \cdot [ADTT(year\ built)] \cdot \frac{(1 + GF_1)^n - 1}{GF_1} \qquad (2.10)$$

Knowing this and the future growth factor, GF_2, the remaining fatigue life in years, R, is

$$R = \frac{\ln\left[\frac{(N - M) \cdot GF_2}{365 \frac{days}{year} \cdot ADTT(n_2) \cdot (1 + GF_2)} + 1\right]}{\ln(1 + GF_2)} \qquad (2.11)$$

This is derived from the engineering economy equation for compound amount.

The following is a general outline of the fatigue evaluation method as presented in BAR7.

1. Obtain the allowable stress range, F_{sr}, from the AASHTO *Specifications* table 10.3.1A for over 2,000,000 cycles.
2. Determine the distribution factor, DF_1, for one lane from the AASHTO *Specifications* table 3.23.1.
3. Calculate the design fatigue stress range, $(f_{sr})_D$, at the detail,

$$(f_{sr})_D = \frac{(M_{live} \cdot DF_1) \cdot y}{I} \qquad (2.12)$$

The M_{live} equals the maximum algebraic difference between the positive live load moment and the negative live load moment multiplied by the impact factor, I_f. The impact factor can be determined as follows from the AASHTO *Specifications*, section 3.8,

$$I_f = \frac{50}{L+125} \leq 0.30 \qquad (2.13)$$

where L is the span length. Live load moment is calculated using the HS20 truck shown in Fig. 2.2. Finally, in Eq. 2.12, y is the distance from the neutral axis of the section to the location of the detail and I is the moment of inertia of the section.

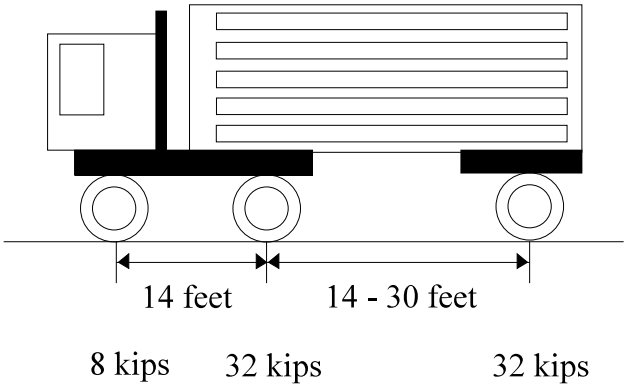

Fig. 2.2 HS20 Truck, AASHTO *Specifications*

4. Infinite life, $(f_{sr})_D \cdot PTF \leq F_{sr}$. If not, proceed to the next step. The Pennsylvania traffic factor, *PTF*, is equal to 1.0 for *ADTT* less than or equal to 2500 and 1.1 if greater than this for one direction.
5. Determine γ. If the gross vehicle weight distribution data is entered, γ is calculated according to the Design Manual part 4. Otherwise, γ equals 0.7 multiplied by the *PTF*

factor. If the gross vehicle weight distribution data is not entered, then,

$$\gamma = 0.7 \cdot PTF \tag{2.14}$$

6. Calculate the effective fatigue stress range, $(f_{sr})_e$,

$$(f_{sr})_e = \gamma \cdot \alpha \cdot (f_{sr})_D \tag{2.15}$$

α equals 0.5 since BAR7 uses the conventional method of structural analysis.

7. Obtain constant *A* from the Design Manual part 4, table P5.1.1.1.1.3(A). This is according to the AASHTO fatigue category for the specified detail.

8. Calculate the design fatigue life in cycles, *N*,

$$N = \frac{A}{(f_{sr})_e^3} \tag{2.9}$$

9. Calculate the remaining fatigue life, *R*, in years, following steps a, b, c, and d below:

   a. Determine the past growth factor, GF_1. This may be estimated or calculated by BAR7 provided that the *ADTT* value for two separate years are known.

$$GF_1 = \sqrt[n_3]{\frac{ADTT(n_2)}{ADTT(n_1)}} - 1 \tag{2.16}$$

   n_1 = previous year
   n_2 = recent year
   $n_3 = n_2 - n_1$

   b. Calculate the *ADTT* for the year the bridge was built,

$$ADTT(year\ built) = \frac{ADTT(n_2)}{(1+GF_1)^n} \tag{2.17}$$

   $n = n_2 - year\ built$

   c. Calculate the number of cycles, *M*, accumulated up to year n_2,

$$M = 365 \frac{days}{year} \cdot [ADTT(year\ built)] \cdot \frac{(1 + GF_1)^n - 1}{GF_1} \qquad (2.10)$$

$n = n_2$ - *year built*

d. Determine the future growth factor, GF_2. This may be estimated or calculated by BAR7 provided that the estimated *ADTT* for the future year, n_f, is entered.

$$GF_2 = \sqrt[n_4]{\frac{ADTT(n_f)}{ADTT(n_2)}} - 1 \qquad (2.18)$$

$n_4 = n_f - n_2$

e. Calculate the remaining fatigue life, *R*, in years,

$$R = \frac{\ln\left[\frac{(N - M) \cdot GF_2}{365 \frac{days}{year} \cdot ADTT(n_2) \cdot (1 + GF_2)} + 1\right]}{\ln(1 + GF_2)} \qquad (2.11)$$

2.4 Lehigh Method

Like BAR7, the Lehigh method is applicable to steel girder and truss type bridges of short to medium span with redundant or non-redundant members.

In this method, the maximum range in live load stress is called the maximum stress range. This may be found from the various procedures mentioned previously such as stress histograms, weigh-in-motion measurements near the site, or using BAR7 with the HS20 truck. It also may be calculated from the same simple stress, σ, equation. As with BAR7, the moment is determined using the HS20 truck. Both the impact factor and the distribution factor are determined as

described in BAR7.

Fatigue life analysis is based on the same equation which is consistent with Miner's law,

$$N = \frac{c_f}{S_R^3} \tag{2.8}$$

Results are graphical. The accumulated number of cycles and effective fatigue stress range are plotted on the same graph as the *SN* curve for the specified AASHTO fatigue category. The relative position of this point and the respective fatigue resistance curve provide an estimation of the cumulative fatigue damage and the remaining fatigue life. "When the number of cycles accumulated reaches 80 to 90 percent of the distance of the fatigue resistance curve, visible cracking should be apparent and detectable." (Fisher, Yen, and Wang 1989).

The following is a general outline of the fatigue evaluation method as presented by Lehigh University.

1. Obtain the allowable stress range, F_{sr}, from the AASHTO *Specifications* table 10.3.1.A for over 2,000,000 cycles.
2. Determine the distribution factor, DF_1, for one lane from the AASHTO *Specifications* table 3.23.1.
3. Determine the maximum stress range, S_{rmax}, at the detail,

$$S_{rmax} = \frac{(M_{live} \cdot DF_1) \cdot y}{I} \tag{2.19}$$

To evaluate this expression see BAR7, step 3.

4. Infinite life if, $S_{rmax} < F_{sr}$. If not, proceed to the next step.
5. Obtain the actual maximum stress range, S_{rmax}. This may be determined from information on gross vehicle weight plus impact from local weigh stations or by a stress range histogram. Finite elements may also be used to determine S_{rmax}.
6. Infinite life if, $S_{rmax} < F_{sr}$. If not proceed to the next step.
7. Compute the effective fatigue stress range, S_{re},

$$S_{re} = [\sum \gamma_i \cdot S_{ri}^3]^{1/3} \quad (2.20)$$

This is Miner's law where γ_i is the percentage frequency of occurrence of stress range, S_{ri}.

8. Determine the accumulated number of cycles, N_T,

$$N_T = \textit{one-way ADTT} \cdot \textit{number of days the bridge has been in service} \quad (2.21)$$

9. Plot N_T, S_{re} on the respective *SN* curve. As mentioned before, the relative position of this point and the respective fatigue resistance curve provide an estimation of the cumulative fatigue damage and the remaining fatigue life.

2.5 Linear Elastic Fracture Mechanics (LEFM)

Like the AASHTO *Guide Specifications*, LEFM can be used for fatigue evaluations of steel bridges with redundant or nonredundant members. It is noted that the AASHTO Guide Specification is applicable for uncracked members but LEFM is also applicable to cracked members so long as the crack is small in size.

In order for fatigue fracture to occur, a crack must be present. First, the crack is initiated. This can occur as a result of fabrication stresses, construction stresses, or initial service stresses. Propagation of this initial crack to fracture occurs due to the range of tensile cyclic stress, stress

concentration, the type and shape of the crack, the properties of the material, and other factors.

LEFM assumes that the majority of fatigue life occurs during crack propagation, rather than initiation. It relates the distribution and magnitude of the stress field near the crack tip to the nominal stress range applied to the structural member. Tension stress paths appear as follows demonstrating that stresses are concentrated near the crack tip.

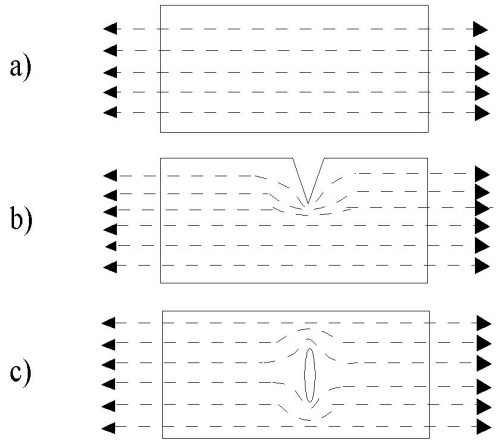

Fig. 2.3 Stress Paths: a) Uncracked Bar, b) Edge Cracked Bar, and c) Interior Surface Cracked Bar

For metals, there are three regions which describe the behavior of fatigue crack propagation. In region I, there is a fatigue threshold, K_{th}, Fig. 2.4. Below this, cracks do not propagate. Region II represents linear fatigue crack propagation. This region can be described by the following equation,

$$\frac{da}{dN} = C \cdot \Delta K^{m} \qquad (2.22)$$

C and *m* are constants which depend on: material variables, environment, load frequency, temperature, and the applied stress range. In region III, acceleration of crack growth results from local fracture as K_{max} approaches K_c, the fracture toughness of the metal (Hertzberg 1989). ΔK is the stress intensity factor, and it is a function of the properties of the metal, the crack orientation, as well as the size and shape of the crack.

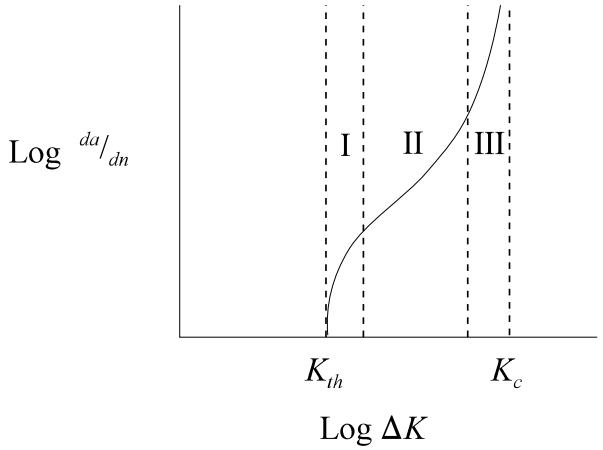

Fig. 2.4 Fatigue Crack Growth Versus Stress Intensity Factor Range

For an infinite plate with a central through crack, the stress intensity factor is defined as,

$$K = \sigma \cdot \sqrt{\pi \cdot a} \qquad (2.23)$$

σ is the axial stress, and *a* is the crack length. Factors are then used to modify this for other types of cases where crack geometry and specimen geometry are different. These factors account for a stress gradient acting near the crack tip, finite width or thickness of the member, a free surface, and

a three dimensional crack. These factors vary depending on the type of detail.

For a net tensile, cyclic fatigue loading due to truck traffic, $\Delta\sigma$ is the live load stress range which results in a ΔK, stress intensity factor range. (Herein, $\Delta\sigma$ is S_r, the nominal stress range in accordance with the AASHTO *Guide Specifications*.) Knowing the stress intensity factor range as well as constants C and m, the number of cycles to fracture can be calculated using an equation which describes region II, crack propagation. This relationship repeated from above is,

$$\frac{da}{dN} = C \cdot \Delta K^m \tag{2.22}$$

Which can be solved for the total fatigue life in cycles, N,

$$N = \frac{1}{C} \cdot \int_{a_i}^{a_{cr}} \frac{1}{\Delta K^m} da \tag{2.24}$$

where a_i is the initial crack length which is typically taken as the largest permissible flaw as guaranteed by the manufacturer, a_{cr} is the critical crack length which can be determined knowing the critical stress intensity factor, K_{Ic}, for the plane strain condition.

Once the total fatigue life in cycles is calculated, the BAR7 procedure may be used to determine the remaining fatigue life in years.

The following is a general outline of the fatigue evaluation method using LEFM:

1. Determine the critical stress intensity factor for plane strain condition, K_{Ic}, corresponding to the minimum service temperature. Having determined the minimum service temperature, K_{Ic} can be found in various metals handbooks.
2. Determine if the member is in a state of plane strain. It is, if the detail meets the following

conditions,

$$a \geq 2.5 \cdot \left(\frac{K_{Ic}}{\sigma_{ys}}\right)^2 \quad t \geq 2.5 \cdot \left(\frac{K_{Ic}}{\sigma_{ys}}\right)^2 \quad w \geq 5.0 \cdot \left(\frac{K_{Ic}}{\sigma_{ys}}\right)^2 \qquad (2.25,\ 2.26,\ 2.27)$$

σ_{ys} is the plane strain yield strength. It equals $\sqrt{3} \cdot$ uniaxial plane stress yield strength. a, t, and w correspond to the crack length, member thickness and member width, respectively. If the detail does not meet the above conditions, it is in a state of plane stress. Other methods of analysis which are not considered here must be used such as: R-curve analysis, crack tip opening displacement, J integral, or tearing modulus.

For steel bridge applications, LEFM is usually sufficient (Fisher 1984). However, other sources disagree stating that crack initiation can be a substantial portion of the total fatigue life (Shilling, et. al. 1978). While this is an area of debate, neglecting crack initiation is conservative. At low stress levels, LEFM can be used safely and conservatively (Collacott 1985). Most details of existing steel bridges experience a maximum range of live load stress that is relatively low. This range is well below the yield strength of the steel. This range rarely exceeds 5 ksi and is usually between 1 to 3 ksi (Moses, Schilling, and Raju 1987). Therefore, the use of LEFM for the evaluation of crack propagation potential at details of existing steel bridges is justified.

3. Determine the initial crack length, a_i. This should be taken as the largest permissible flaw as guaranteed by the manufacturer.

4. Having met the plane strain requirements of step 2, determine the critical crack size, a_{cr}, from the following equation,

$$K_{Ic} = F_s \cdot F_w \cdot F_g \cdot F_e \cdot \sigma_{peak} \cdot \sqrt{\pi \cdot a_{cr}} \quad (2.28)$$

The factors F_s, F_w, F_g, and F_e modify the case with an infinite plate subjected to a varying uniform tensile stress with a central through crack to account for the particular case in question. F_s is the free surface correction factor used for a semi-elliptical crack in a semi-infinite plate subjected to the uniform stress range. The finite width or thickness correction, F_w, accounts for a central crack in a plate of finite width. The stress gradient correction factor, F_g, accounts for nonuniform, nominal stresses acting near the crack. Finally, the elliptical crack shape correction, F_e, transforms a two dimensional crack to a three dimensional crack.

5. Determine the total fatigue life in cycles, N, for the nominal stress range, S_r from,

$$\frac{da}{dN} = C \cdot \Delta K^m \quad (2.22)$$

Using the technique of separation of variables from differential equations, the total fatigue life in cycles, N, may be calculated as,

$$N = \frac{1}{C} \cdot \int_{a_i}^{a_{cr}} \frac{1}{\Delta K^m} da \quad (2.24)$$

where,

$$\Delta K = F_s \cdot F_w \cdot F_g \cdot F_e \cdot S_r \cdot \sqrt{\pi \cdot a} \quad (2.29)$$

S_r is the maximum stress range due to live load. In this report, it will be determined in

accordance with the AASHTO *Guide Specifications*. Factors F_s, F_w, F_g, and F_e are the same as ones determined in step 4.

Structural members are primarily made up of mild steel. For these types, m equals 3.0. C is $3.6 \cdot 10^{-10}$ using units of inches for crack size and ksi$\sqrt{\text{in}}$ for ΔK. This is the upper bound value for structural steels and welds in these steels, excluding A514 steel (Barsom and Rolfe 1987). The average crack growth constant is $2.05 \cdot 10^{-10}$ using units of inches for crack size and ksi$\sqrt{\text{in}}$ for ΔK (Fisher and Hirt 1973). Although Fisher in much of his fracture mechanics work used the upper bound value for the crack growth constant, Zhao et. al. (1994) used the average value instead. The average crack growth constant will be used.

$$N = \frac{1}{2.05 \cdot 10^{-10}} \int_{a_i}^{a_{cr}} \frac{1}{(F_s \cdot F_w \cdot F_g \cdot F_e \cdot S_r \cdot \sqrt{\pi \cdot a})^{3.0}} da \qquad (2.30)$$

6. See step 9 of BAR7 to determine the remaining fatigue life, R, in years.

2.6 Examples

The following two examples demonstrate the use of the four fatigue life methods, i.e. the AASHTO *Guide Specifications*, BAR7, the Lehigh method, and LEFM. The details are typical in the sense that there is no site specific data available with the exception of traffic data. The first detail is a welded cover plate on an interior girder. This is a classical case having an AASHTO fatigue category of E'. The second detail is a welded web connection on an interior girder. While the AASHTO fatigue category is only C, the example demonstrates a detail with infinite fatigue life.

2.7 Welded Cover Plate End, Detail No. 1

Bridge number 453 consist of a series of eight simple spans and is located in Cranston, Rhode Island. Built in 1959, the steel bridge is a multi-girder type. The first span is 54 feet long. The interior girders for span one are W33x130 members. Attached to the bottom of the girders are 0.375 inch cover plates. The fatigue strength of the cover plate girders with flange thickness greater than 0.800 inches have the lowest AASHTO fatigue rating, category E'. Since the flange thickness for a W33x130 is 0.855 inches, the AASHTO fatigue category is E'. The average girder spacing is 6.42 feet. The construction is composite and there is no haunch.

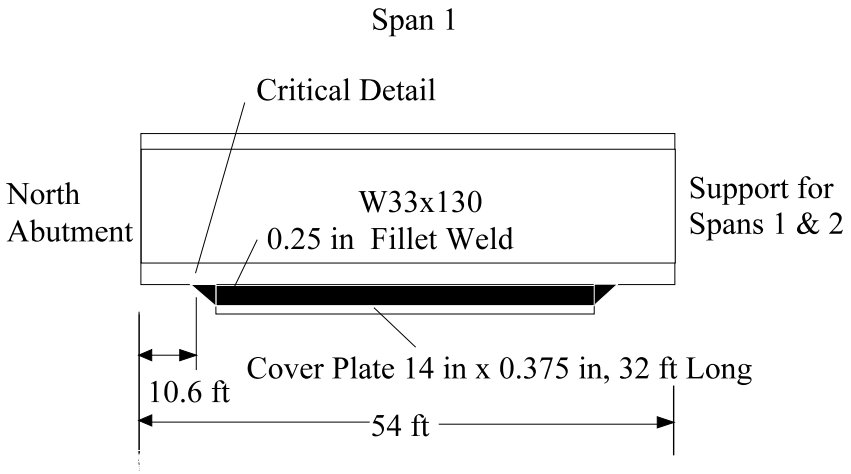

Fig. 2.5 Welded Cover Plate Girder, Detail No. 1

2.7.1 AASHTO Guide Specifications

The following is the evaluation of the remaining fatigue life using the **AASHTO *Guide Specifications***. All section references, unless noted otherwise, refer to the AASHTO Guide Specifications for Fatigue Evaluation of Existing Steel Bridges, Interim 1993. It is noted that the detail under consideration, end of cover plate, is at 10.6 ft from the support.

1) The limiting stress range for a Detail E', S_{FL}, equals 0.9 ksi, from section 3.3.

2) The nominal stress range at the detail is:

$$S_r = \frac{(M_{live} \cdot DF) \cdot y}{I} \qquad (2.5)$$

The maximum live load moment, M_{live}, is found using using the fatigue truck from Fig. 2.2A. The impact factor is 1.10 for smooth pavement conditions in accordance with section 2.4. The span is simply supported. Therefore, the maximum negative live load moment is zero. The maximum positive bending moment at the detail under consideration occurs when the heaviest axle load is placed directly at the critical location. The positions of the other axles is set by axle spacing. The maximum live load moment at the detail occurs when the fatigue truck is placed as shown in Fig. 2.6. The resulting maximum live load moment at 10.6 feet from the left support is 294 k-ft.

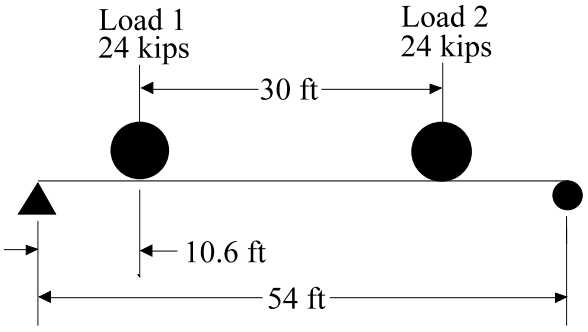

Fig. 2.6 Location of Fatigue Truck Resulting in Maximum Live Load Moment at Detail No. 1

The lateral distribution factor must be determined. This depends on the span length, the

location along the span, the percentages of different types of trucks in traffic, and the type of bridge span i.e. whether it is simple or continuous. From section 2.6.1, the lateral distribution for I-shaped, interior members is $DF_i = S/D$. The girder spacing S is 6.42 ft. The factor D is found to be 19.7 using linear interpolation from Section 2.6.1. Substituting, the distribution factor is:

$$DF_i = S/D = 6.42 \text{ ft}/19.7 = 0.326 \quad (< (S - 3)/S = 0.533)$$

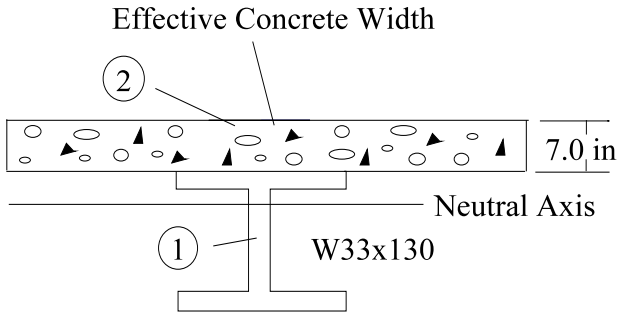

Fig. 2.7 Composite Concrete Bridge Deck, Detail No. 1

Fig. 2.7 shows the geometry of the cross section. It is noted that according to AASHTO *Specifications*, section 10.38.3.1, the effective flange width of the concrete is the girder spacing which is 6.42 feet. The distance y between the neutral axis and the detail is 29.2 inches. The total moment of inertia for sections 1 and 2 is,

$$I_T = 16{,}800 \text{ in}^4$$

An additional factor of 1.15 is used since there is composite action in the concrete deck, see section 2.7.1. The nominal stress range is:

$$S_r = \frac{(294 \cdot 12 \cdot 0.326) \cdot 29.2}{16{,}800} \cdot \frac{1}{1.15}$$

$$S_r = 1.74 \text{ ksi}$$

3) $$R_S = R_{S0} \cdot F_{S1} \cdot F_{S2} \cdot F_{S3} \qquad (2.6)$$

$R_{S0} = 1.35$ This is a redundant member.
$F_{S1} = 1.0$ No measurements.
$F_{S2} = 1.0$ Standard fatigue truck used.
$F_{S3} = 1.0$ Normal procedure used.

$$R_S = 1.35$$

4) $1.35 \cdot S_r > 0.9$ Therefore, the fatigue life is finite.

5) The remaining safe fatigue life is:

$$Y_f = \frac{f \cdot K \times 10^6}{T_a \cdot C \cdot (R_S \cdot S_r)^3} - a \qquad (2.7)$$

f = 1.0 safe life
K = 1.1 from table in section 3.3
$T_a = 1.3 \cdot 1538 = 2000$
1.3 comes from figure 3.5A, where the annual growth rate, g, is 5 %
$1538 = ADT \cdot F_T \cdot F_L$
ADT = 36,196 from traffic data
F_T = 0.05 fraction of trucks
F_L = 0.85 fraction of trucks in outer lane, see table in section 3.5. with number of lanes = 2, 1-way traffic.
C = 1.0 cycles per truck passage. See section 3.4 for longitudinal members, simple span girders 40 feet or more.
a = 34 years, present age of bridge

$$Y_f = \frac{1.0 \cdot 1.1 \times 10^6}{2000 \cdot 1.0 \cdot (1.35 \cdot 1.74)^3} - 34$$

Y_f = 8.5 remaining **safe** fatigue years

Remaining mean fatigue life,

$$Y_f = \frac{f \cdot K \times 10^6}{T_a \cdot C \cdot (R_S \cdot S_r)^3} - a \qquad (2.7)$$

$f = 2.0$
$R_S = 1.0$
All other factors are the same as the safe fatigue life calculation.

$$Y_f = \frac{2.0 \cdot 1.1 \times 10^6}{2000 \cdot 1.0 \cdot (1.00 \cdot 1.74)^3} - 34$$

$Y_f = 175$ remaining **mean** fatigue years

2.7.2 Fatigue Prediction Using BAR7

The same example is here studied using BAR7.

1) F_{sr} equals 2.6 ksi, from AASHTO *Specifications* table 10.3.1.A.

2) DF_1 = S/5.5 wheels = 6.42 ft/5.5 wheels = 6.42 ft/(5.5·2) axles = 0.584, AASHTO *Specifications* table 3.23.1.

3) The design fatigue stress range at the detail is

$$(f_{sr})_D = \frac{(M_{live} \cdot DF_1) \cdot y}{I} \qquad (2.12)$$

The impact factor from formula 3-1 of AASHTO *Specifications* section 3.8.2.2 (a) is,

$I_f = 50/(L + 125) = 50/(54 \text{ ft} + 125) = 0.28 \leq 0.30$

Where L is the span length. For the maximum live load moment, the same procedure is used as in the previous section. The difference is that now the axle loads are 32 kips each instead of 24 kips. The final maximum live load moment including impact is 457 k-ft. It is noted that a 30 ft spacing of the rear axles is used .

From before, $y = 29.2$ in, and $I_T = 16{,}800$ in^4. Then the stress range becomes:

$$(f_{sr})_D = \frac{457 \cdot 12 \cdot 0.584 \cdot 29.2}{16{,}800}$$

$$(f_{sr})_D = 5.57 \text{ ksi}$$

4) The Pennsylvania traffic factor, *PTF*, equals 1.0 for *ADTT* less than or equal to 2500. The *ADTT* for 1993 is 1810. Therefore,

$$5.57 \text{ ksi} \cdot PTF = 5.57 \text{ ksi} > F_{sr} = 2.6 \text{ ksi}$$

and the detail has a finite life.

5) $\gamma = 0.7 \cdot PTF = 0.7$

6) $(f_{sr})_e = \gamma \cdot \alpha \cdot (f_{sr})_D = 0.7 \cdot 0.5 \cdot 5.57 \text{ ksi} = 1.95 \text{ ksi}$

7) A is a constant from the Design Manual part 4, table P5.1.1.1.1.3(A) which depends on the AASHTO fatigue category, A=37E10^6. This constant is needed to determine the design fatigue life in cycles, N, see step 8. An alternative way to determine N is to use the AASHTO fatigue design curves. Since the design fatigue stress range, $(f_{sr})_D$, is known, the design fatigue life in cycles may be determined directly from the AASHTO fatigue design curves. Since $(f_{sr})_D$ equals 5.57 ksi, N corresponds to 5,000,000 cycles.

8) $N = \frac{A}{(f_{sr})_e^3} \approx \mathbf{5{,}000{,}000}$ design fatigue life in cycles

9) Calculate the remaining fatigue life in years, R. Note that the bridge was built in 1959.

$GF_1 = 0.05$ past growth factor $\qquad$ $n = 1993 - 1959 = 34$ years

$$ADTT_{1993} = 1810$$

$$ADTT_{1959} = \frac{ADTT_{1993}}{(1 + GF_1)^n} = 345$$

$$M = 365 \frac{days}{year} \cdot [ADTT_{1959}] \cdot \frac{(1 + GF_1)^n - 1}{GF_1} \qquad (2.10)$$

$M = 10{,}700{,}000$ accumulated cycles

Since $M > N$, the fatigue life is 0 remaining years. Therefore,

$R = 0$ remaining years

2.7.3 Lehigh Method

The remaining fatigue life of detail No. 1 is now calculated using the Lehigh method.

1) F_{sr} equals 2.6 ksi, same as BAR7.

2) DF_1 equals 0.584, same as BAR7.

3) S_{rmax} equals 5.57 ksi, same as BAR7 except the variable is called $(f_{sr})_D$.

4) Infinite life if, $S_{rmax} < F_{sr}$.

$$5.57 \text{ ksi} > 2.6 \text{ ksi}$$

The fatigue life is finite.

5) No available data to determine the maximum stress range, S_{rmax}, more accurately exists.

6) The effective fatigue stress range, S_{re}, cannot be determined. There is no other available data.

7) Determine the accumulated number of cycles, N_T,

$$N_T = \textit{one-way ADTT} \cdot \textit{number of days the bridge has been in service} \quad (2.21)$$

This is a poor equation since *ADTT* usually increases considerably during the life of the bridge. From BAR7,

$$N_T = 10{,}700{,}000 \text{ accumulated cycles}$$

The Lehigh method for fatigue evaluation is primarily a graphical procedure. The *SN* curve for the particular detail is graphed. Also, the point representing the accumulated number of cycles and the effective fatigue stress range (N_T, S_{re}) is plotted. In this case, the line representing the accumulated number of cycles is plotted. The relative positions indicate the remaining fatigue life, see Fig. 2.8. It is important to remember that this is a log-log plot.

In this case, since the effective stress range is not available, one can use the maximum stress range which would indicate that the fatigue life for this detail has been exhausted .

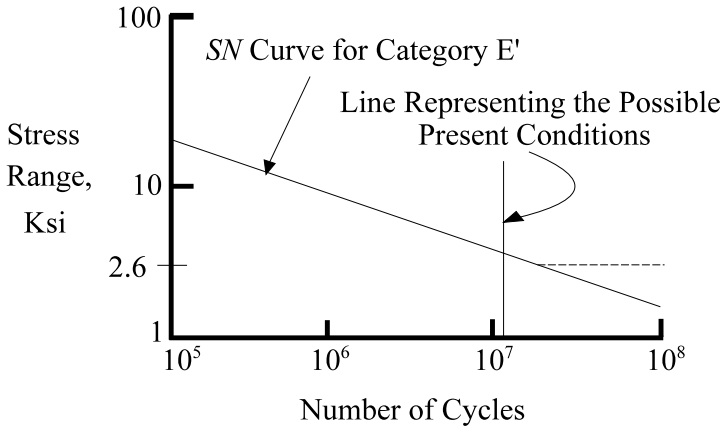

Figure 2.8 Stress Range Versus Number of Cycles,
Detail No. 1

2.7.4 LEFM Method

Finally, the remaining fatigue life is calculated for detail No. 1 using LEFM. The geometry of cracks that form at the toe of weld are highly irregular but are most often modeled as semi-elliptical (Fisher 1984). Therefore, the crack is modeled as a semi-elliptical surface crack oriented perpendicular to the direction of stress. The semi-elliptical crack initiates and then propagates from the toe of the weld because large localized stresses exist. In addition to this, there is a change in geometry where the cover plate abruptly ends. Also, there is a change in homogeneity at the toe of the weld from the A36 steel to the weld material.

The following is a diagram of a semi-elliptical crack. c represents the crack shape or half of the length of the crack which is perpendicular to the live load stress range, S_r. This direction is along the edge of the welded toe.

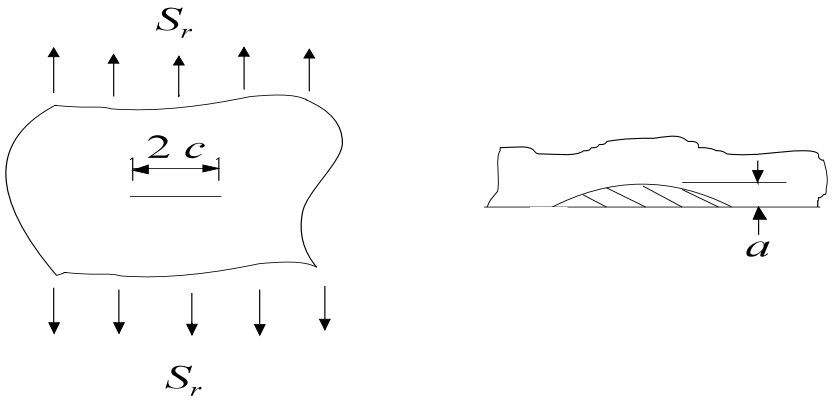

Figure 2.9 Semi-elliptical Surface Crack, Detail No. 1

The initial crack depth, a_i, and critical crack depth, a_{cr}, are crucial parameters. For AASHTO fatigue category E details, the mean initial crack length is approximately 0.02 inch for a lognormal distribution (Albrecht and Yazdani 1986). "Under extreme prior fatigue-loading conditions, which far exceed those usually encountered in actual bridges, cracks developed at the cover plate ends and ranged in depth from 0.03 to 0.375 inch. In service, members with cracks about 0.40 inch deep would soon fail by fatigue regardless of the level of fracture toughness of the steel." (Barsom and Rolfe 1987). From this,

a_i = 0.02 inch initial crack depth

a_{cr} = 0.40 inch critical crack depth

The crack shape, c, can be determined from (Fisher 1984),

$$c(a) = 5.457 \cdot a^{1.133} \text{ inch} \tag{2.31}$$

This is conservative given that this is the lower bound. The total fatigue life in cycles, N, is:

$$N = \frac{1}{2.05 \cdot 10^{-10}} \int_{a_i}^{a_{cr}} \frac{1}{(F_s \cdot F_w \cdot F_g \cdot F_e \cdot S_r \cdot \sqrt{\pi \cdot a})^{3.0}} da \tag{2.30}$$

S_r equals 1.74 ksi. This is the nominal stress range, S_r, as calculated previously in the AASHTO *Guide Specifications* approach. The correction factors, F_s, F_w, F_g, and F_e for a welded cover plate are given below (Fisher 1984). It is noted that α is the variable of integration.

$$F_s = 1.211 - 0.186 \cdot \sqrt{\frac{a}{c(a)}} \tag{2.32}$$

$$F_w = \sqrt{\sec \frac{\pi \cdot a}{2 \cdot b}} \tag{2.33}$$

$2 \cdot b$ represents the flange width. For a W33x130, the flange width is 11.510 inches.

$$F_g = \frac{-3.539 \cdot \ln \frac{Z}{t_f} + 1.981 \cdot \ln \frac{t_{cp}}{t_f} + 5.798}{1 + 6.789 \cdot (\frac{a}{t_f})^{0.4348}} \tag{2.34}$$

Z is the weld leg size. Given a W33x130 member with a flange thickness, t_f, of 0.855 inches and a cover plate with a thickness, t_{cp}, of 0.375 inch, the weld leg size can be estimated from maximum and minimum weld sizes as 0.313 inch (Blodgett 1968)

$$F_e = \frac{1}{\int_0^{\frac{\pi}{2}} \sqrt{1 - \frac{c(a)^2 - a^2}{c(a)^2} \cdot \sin^2(\theta)}\, d\theta} \qquad (2.35)$$

Having defined all of the variables in Eq. 2.30, the total fatigue life in cycles is found by numerical integration as $N = 97{,}200{,}000$ cycles

Now that the total fatigue life in cycles has been determined, the remaining fatigue life in years can be determined using the BAR7 approach.

$GF_1 = 0.05$ past growth factor

$n = 1993 - 1959 = 34$ years

$ADTT_{1993} = 1810$

$$ADTT_{1959} = \frac{ADTT_{1993}}{(1 + GF_1)^n} = 345$$

$$M = 365 \frac{days}{year} \cdot [ADTT_{1959}] \cdot \frac{(1 + GF_1)^n - 1}{GF_1} \qquad (2.10)$$

$M = 10{,}700{,}000$ accumulated cycles

$GF_2 = 0.05$ future growth factor

$$R = \frac{\ln\left[\frac{(N - M) \cdot GF_2}{365 \frac{days}{year} \cdot ADTT_{1993} \cdot (1 + GF_2)} + 1\right]}{\ln(1 + GF_2)} \qquad (2.11)$$

R = 40.6 remaining years

To demonstrate that this approach is valid, a plot is made using equation (2.30) of the stress range versus the number of cycles. This plot is then compared to Fig. 2.8 showing the AASHTO fatigue curve for fatigue category E', Fig, 2.8. The graphs are very similar.

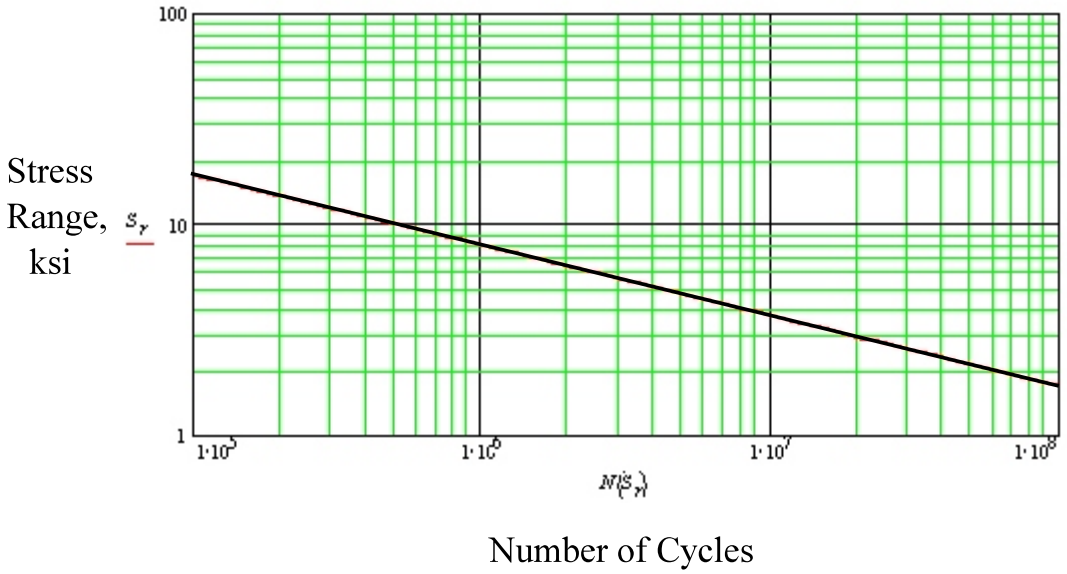

Fig. 2.10 Stress Range Versus Number of Cycles using LEFM, Detail No. 1

Fig. 2.11 shows the results in years for all four methods in a simple timeline. Notice how conservative the BAR7 approach is for this particular example.

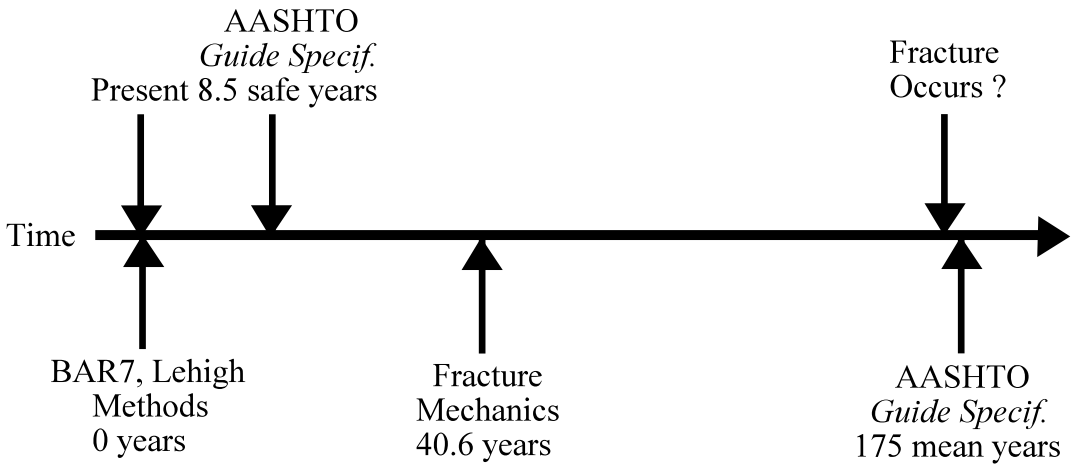

Fig. 2.11 Summary of Remaining Fatigue Life for Detail No. 1

2.8 Welded Web Connection, Detail No. 2

Bridge number 667 consist of a series of three simple spans, located in Providence, Rhode Island. Built in 1964, the steel bridge is a multi-girder type. Span two is 82.8 feet. The interior girders for span two are W36x170 members. The average stringer spacing is 6.77 feet. The concrete deck acts as a composite. A welded web connection is located at midspan at 19.44 in from the bottom of the section, see Fig. 2.12 for an out of scale schematic. Please note that Fig. 2.12 shows an empty space in the location of a 2 in haunch since it is not used for the structural capacity of the section. This detail is a transverse member connection to the web of a girder with an AASHTO fatigue category rating of C. The top flange is continuously braced.

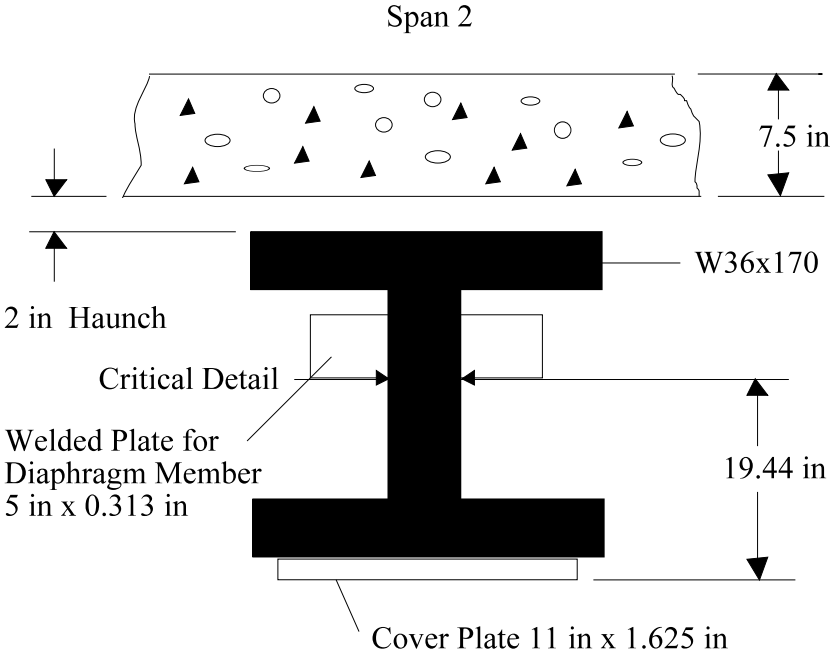

Figure 2.12 Welded Web Connection, Detail No. 2

The fatigue life of this detail is evaluated using the four procedures described earlier.

2.8.1 AASHTO Guide Specifications

1) S_{FL} equals to 3.7 ksi, from section 3.3 (Detail Category C).

2) The nominal stress range at the critical location is

$$S_r = \frac{(M_{live} \cdot DF) \cdot y}{I} \qquad (2.5)$$

The impact factor is 1.25 for fairly rough pavement conditions in accordance with section 2.4. The negative live load moment is zero since the span is simply supported. The maximum

positive live load moment at midspan (where the detail is located) occurs when the fatigue truck is placed in the location shown at Fig. 2.13. It is found to be 891 k-ft.

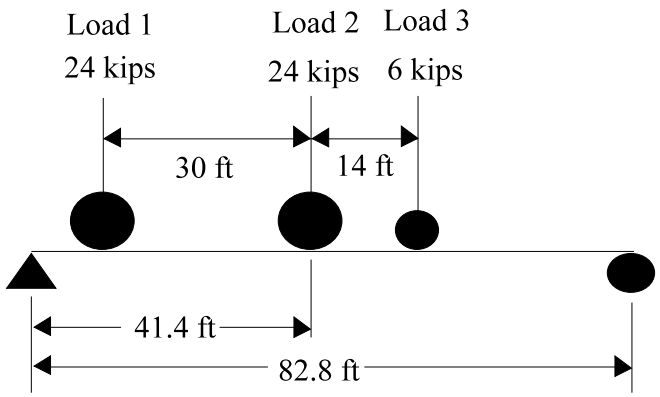

Fig. 2.13 Location of Fatigue Truck Resulting in Maximum Live Load Moment at Detail No. 2

The distribution factor for one lane is $DF_i = S/D$. S equals 6.77 feet, girder spacing. D is found by interpolation in section 2.6 to be 21.5. Therefore,

$$DF_i = 6.77 \text{ ft}/21.5 = 0.315 \quad (< (S - 3)/S = 0.557)$$

According to the AASHTO *Specifications*, section 10.38.3.1, the controlling effective flange width of the concrete is the girder spacing, i.e. 6.77 feet. The neutral axis of the transformed section shown in Fig. 2.14 is located 30 in from the very bottom. The distance y between the neutral axis and the detail is 30-19.4=10.6 inches. The total inertia of the section is $I_T = 45{,}400 \text{ in}^4$.

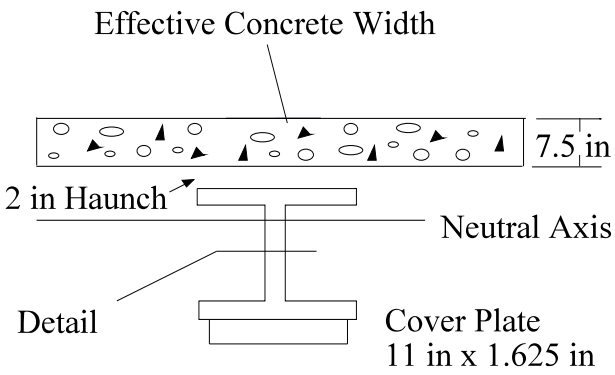

Figure 2.14 Composite Concrete Bridge Deck, Detail No. 2

By including a factor of 1.15 from section 2.7.1 for composite construction the nominal stress range becomes

$$S_r = \frac{(891 \cdot 12 \cdot 0.315) \cdot 10.6}{45{,}400} \cdot \frac{1}{1.15}$$

$$S_r = 0.684 \text{ ksi} << S_{FL} = 3.7 \text{ ksi}$$

This indicates that the fatigue life is infinite.

2.8.2 Fatigue Prediction Using BAR7

The same example is now done using the BAR7 approach.

1) F_{sr} equals 16 ksi, from AASHTO *Specifications* table 10.3.1.A.

2) $DF_1 = S/5.5$ wheels = 6.77 ft/5.5 wheels = 6.77 ft/(5.5·2) axles = 0.615, AASHTO *Specifications* table 3.23.1.

3) The design fatigue stress range is

$$(f_{sr})_D = \frac{(M_{live} \cdot DF_1) \cdot y}{I} \qquad (2.12)$$

The impact factor from formula 3-1 of AASHTO *Specifications* section 3.8.2.2 (a) is,

$$I_f = 50/(L + 125) = 50/(82.8 \text{ ft} + 125) = 0.24 \leq 0.30$$

L is the span length. The span is simply supported so the maximum negative live load moment is 0 k-ft. To determine the maximum positive live load moment, see the procedure used previously for the AASHTO *Guide Specifications*. This time loads 1 and loads 2 are equal to 32 kips instead of 24 kips, and load 3 is equal to 8 kips instead of 6 kips in accordance with the AASHTO *Specifications*, HS20 truck. The live load moment from load 1 is 182 k-ft, and the live load moment from load 2 is 659 k-ft. The final maximum live load moment at midspan including impact is 1180 k-ft.

$$(182 \text{ k-ft} + 659 \text{ k-ft} + 110 \text{ k-ft}) \cdot (1 + 0.24) = 1180 \text{ k-ft.}$$

From before the distance of the detail from the neutral axis is $y = 10.6$ in and the moment of inertia is $I_T = 45{,}400$ in^4. Then,

$$(f_{sr})_D = \frac{1180 \cdot 12 \cdot 0.615 \cdot 10.6}{45{,}400}$$

$$(f_{sr})_D = 2.03 \text{ ksi}$$

4) The Pennsylvania traffic factor, *PTF*, equals 1.0 for *ADTT* less than or equal to 2500. The *ADTT* for 1993 for this bridge is 1118. Therefore,

$$(f_{sr})_D \cdot PTF = 2.03 \text{ ksi} << F_{sr} = 16 \text{ ksi}$$

and the fatigue life is infinite.

2.8.3 Lehigh Procedure

The remaining fatigue life of detail No. 2 is now calculated using the Lehigh method.

1) F_{sr} equals 16 ksi, same as BAR7.

2) DF_1 equals 0.615, same as BAR7.

3) S_{rmax} equals 2.03 ksi, same as BAR7 except the variable is called $(f_{sr})_D$.

4) Infinite life if, $S_{rmax} < F_{sr}$

$$2.03 \text{ ksi} << 16 \text{ ksi}$$

Therefore, the fatigue life is infinite, Fig. 2.15.

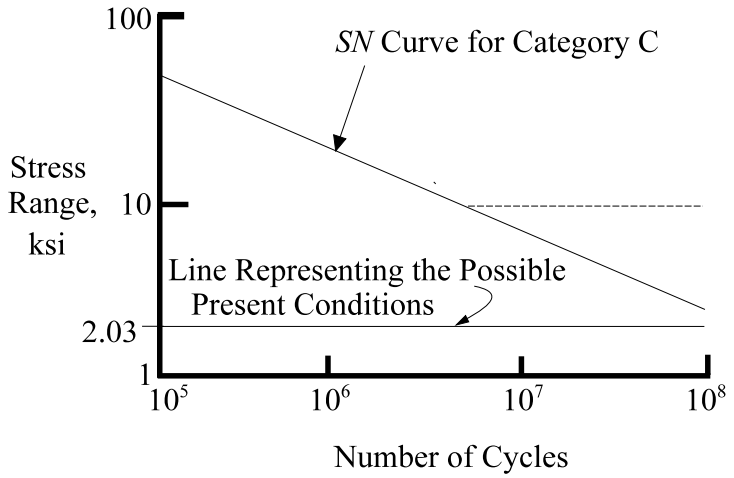

Figure 2.15 Stress Range Versus Number of Cycles, Detail No. 2

2.8.4 LEFM Method

Finally, the remaining fatigue life for detail No. 2 is calculated using LEFM. The crack is modeled as a semi-elliptical surface crack. This is reasonable given that the plate connects to the girders in a perpendicular direction to the stress path such as in the case of the previous example.

This allows for the development of a (semi-elliptical) crack in the web of the girder. Fig. 2.16 presents a schematic where c represents half of the length of the crack which is oriented perpendicular to the live load stress range, S_r.

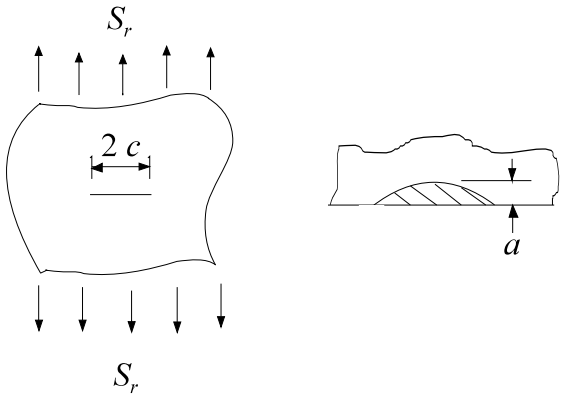

Fig. 2.16 Semi-elliptical Surface Crack, Detail No. 2

For simplicity, the initial and final crack sizes are assumed to be the same as before,

a_i = 0.02 inch initial crack depth

a_{cr} = 0.40 inch final crack depth

The crack shape, c, can be determined from (Fisher 1984),

$$c(a) = 1.197 \cdot a^{0.951} \quad \text{inch} \tag{2.31}$$

The total fatigue life in cycles, N, of this detail needs to be determined. This is given as:

$$N = \frac{1}{2.05 \cdot 10^{-10}} \int_{a_i}^{a_{cr}} \frac{1}{(F_s \cdot F_w \cdot F_g \cdot F_e \cdot S_r \cdot \sqrt{\pi \cdot a})^{3.0}} da \qquad (2.30)$$

S_r equals 0.684 ksi. This is the nominal stress range as calculated previously in the AASHTO *Guide Specifications* approach. The following correction factors, F_s, F_w, F_g, and F_e for an intersecting welded corner are as follows (Fisher 1984),

$$F_s = 1.211 - 0.186 \cdot \sqrt{\frac{a}{c(a)}} \qquad (2.32)$$

$$F_w = \sqrt{\sec \frac{\pi \cdot a}{2 \cdot t}} \qquad (2.33)$$

where t_w represents the web thickness. For a W36x170, the web thickness is 0.680 inches.

$$F_g = 2.64 \cdot [1 - 3.215 \cdot (\frac{a}{t_w}) + 7.897 \cdot (\frac{a}{t_w})^2 - 9.288 \cdot (\frac{a}{t_w})^3 + 4.086 \cdot (\frac{a}{t_w})^4] \qquad (2.38)$$

$$F_e = \frac{1}{\int_0^{\frac{\pi}{2}} \sqrt{1 - \frac{c(a)^2 - a^2}{c(a)^2} \cdot \sin^2(\theta)}\, d\theta} \qquad (2.35)$$

Having defined all of the variables in equation (2.30), the total fatigue life in cycles is found by

numerical integration to be N = 11,000,000,000 cycles. This is a large number but it should be remembered that the stress range is very small and other methods give infinite fatigue life.

Now that the total fatigue life in cycles has been determined, the remaining fatigue life in years will be determined using the BAR7 approach.

GF_1 = 0.028 past growth factor

n = 1993 - 1973 = 20 years

$ADTT_{1993}$ = 1850

$$\mathrm{ADTT}_{1973} = \frac{ADTT_{1993}}{(1 + GF_1)^n} = 1065$$

$$\mathrm{M} = 365\frac{days}{year}\cdot[ADTT_{1973}]\cdot\frac{(1 + GF_1)^n - 1}{GF_1} \qquad (2.10)$$

M = 10,200,000 accumulated cycles

GF_2 = 0.028 future growth factor

$$R = \frac{\ln\left[\frac{(N - M)\cdot GF_2}{365\frac{days}{year}\cdot ADTT_{1993}\cdot(1 + GF_2)} + 1\right]}{\ln(1 + GF_2)} \qquad (2.11)$$

R = 222 remaining years

A plot can be made using equation (2.30) of the stress range versus the number of cycles,

Fig. 2.17. This plot is very similar to Fig. 2.15, the AASHTO fatigue curve for detail C.

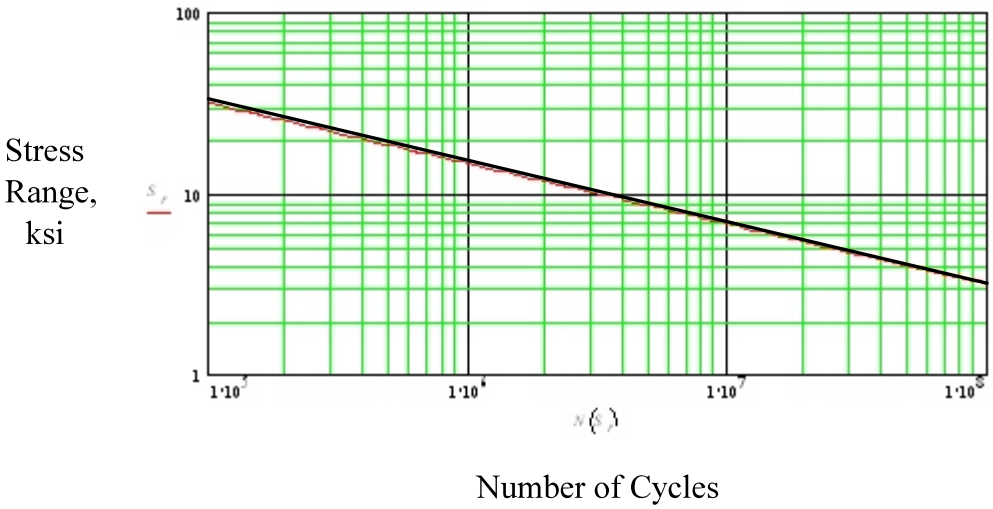

Fig. 2.17 Stress Range Versus Number of Cycles
using LEFM, Detail No. 2

2.9 Comparison of Methods of Evaluating Fatigue Life

Fatigue life predictions using BAR7 are based on design values in the absence of site specific data. Design values are higher than actual values. Although this is conservative, it does not represent the actual fatigue condition of the bridge. As a result, the fatigue life is significantly and unnecessarily reduced.

The Lehigh method is the worst of the four methods. In addition to using design values, the

method gives no definitive way of determining the remaining fatigue life in years. The remaining fatigue life in cycles can be approximated from the *SN* graph comparing the present fatigue condition N_T, S_{re} of the detail with the respective AASHTO fatigue category *SN* curve. However, answers are subjective and in terms of cycles only.

In the AASHTO *Guide Specifications*, approximated truck loads as determined from the fatigue truck are used as opposed to design values. The resulting fatigue life predictions more accurately reflect the fatigue condition of the bridge than the previous methods.

LEFM like the AASHTO *Guide Specifications* uses approximated actual values. This method requires site specific data about the size and type of the detail as well as the crack. If no information is available regarding the crack, its size and type must be assumed.

The four methods of evaluating fatigue have two significant similarities. These include the benefits of incorporating site specific data, and the need to determine the stress range at the detail. While there are only two significant similarities, there are many differences.

Three of the methods are deterministic. They are BAR7, the Lehigh method, and LEFM. The AASHTO *Guide Specifications* is probabilistic.

LEFM is based on fracture mechanics as explained in the previous chapter. The AASHTO *Guide Specifications*, BAR7, and the Lehigh method are all based on Miner's law for fatigue damage. Miner's law is,

$$\sum \frac{n_i}{N_i} = 1 \qquad (3.1)$$

The ratio $\frac{n_i}{N_i}$ is the incremental damage that results from the block of stress ranges, S_{ri}, that occur n_i times. The value N_i corresponds to the constant amplitude cycles to failure at stress range S_{ri}.

Failure is defined when the sum of the increments of damage equals or exceeds unity.

Originally, Miner's law was derived for structural components whose fatigue resistance was governed by crack initiation. Later it was demonstrated to be mainly applicable to components whose fatigue life is governed by crack propagation. Recently, the use of Miner's law as a fatigue damage model has received much attention. Despite arguments as to the validity of Miner's law, tests of simulated bridge members showed that the scatter in predicting the fatigue calculated life is not large (Schilling, et. al. 1978).

Another difference between the methods is the criteria used to determine infinite fatigue life. Also, the calculated stress range used to estimate the remaining fatigue life is different between the methods. The maximum design stress range in both BAR7 and the Lehigh methods is compared with the AASHTO *Specifications* allowable stress range, F_{sr}, to determine possible infinite fatigue life. If the detail has finite life, then these methods determine an effective stress range which is then used to determine the remaining fatigue life. In the AASHTO *Guide Specifications*, the nominal stress range, S_r, is compared to the limiting stress range, S_{FL}, to determine possible infinite fatigue life. If the detail has finite life, the nominal stress range is directly used to determine the remaining fatigue life.

The last major difference is the truck used to determine the stress range if no site specific data is available. In BAR7 and the Lehigh method, this truck is known as the HS20 truck. This is a design vehicle. The AASHTO *Guide Specifications* uses a special fatigue truck. This truck is based on actual truck traffic spectrum from 30 sites nationwide and more than 27,000 observed trucks (Moses, Snyder, and Likins 1985).

Other subtle differences include the impact factor and the distribution factor. In BAR7 and

the Lehigh method, the impact factor is determined in accordance with the AASHTO *Specifications*. To determine this factor just enter the span length, L, into the following equation,

$$I_f = \frac{50}{L + 125} \leq 0.30 \qquad (2.13)$$

The AASHTO *Guide Specifications* uses a different approach based on the condition of the pavement. The moment range may be multiplied by 1.1 to account for smooth surfaces and may be increased up to 1.3 for poor pavement conditions.

The AASHTO *Specifications* lateral distribution factor is the maximum fraction of the axle load that is carried by the longitudinal member under investigation (Moses and Nyman 1984). It is based on all lanes loaded simultaneously. In addition, consideration is given to the worst possible longitudinal location of the truck with respect to the maximum moment. In the AASHTO *Guide Specifications*, the lateral distribution factor accounts only for the portion of the maximum live load moment range carried by the specified member.

All four methods, the AASHTO *Guide Specifications*, BAR7, Lehigh method, and LEFM, are rational methods of fatigue evaluations. BAR7 and the Lehigh method are based on design values in the absence of site specific data. Results based on design values do not adequately reflect actual fatigue conditions. In this study focus is placed on the AASHTO *Guide Specifications* and LEFM since they more accurately determine the actual fatigue conditions in steel bridges. In the following chapter, these two methods are further investigated.

3.0 APPLICATIONS OF AASHTO *GUIDE SPECIFICATIONS* AND LEFM

3.1 Simple Span, Welded Cover Plate Ends

In Rhode Island, many multispan bridges are simply supported. Welded cover ends are the most frequently encountered fatigue prone detail. A typical girder with a welded cover plate is shown in Fig. 3.1.

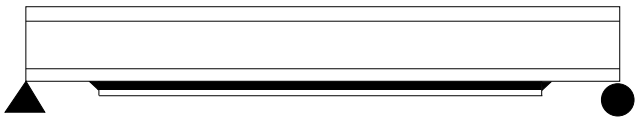

Fig. 3.1 Simply Supported Girder with a Welded Cover Plate

The cover plate does not extend the entire length of the girder since it is used to increase moment capacity. Only the toe of the weld at the cover plate ends are of low fatigue resistance.

Other fatigue prone details in Rhode Island include longitudinal welded web stiffeners in large girders with deep webs, and transverse stiffeners on girders with thin webs. These fatigue prone details are not common, since bridges which contain these details are very old. As a result, most of these bridges have been replaced.

In this chapter, three welded cover plate end details further demonstrate the use of the AASHTO *Guide Specifications* in fatigue calculations. LEFM is also used for comparison purposes. It is realized that some of the calculations are repetitive but they are included in summary form for completeness. The results of these examples as well as the two previous examples from Chapter

2 using the AASHTO *Guide Specifications* and LEFM are discussed in Chapter 4.

3.2 Welded Cover Plate End, Detail No. 3

Bridge number 593 is a simply supported bridge, located on Interstate 95 over Route 3 in Richmond, Rhode Island. Built in 1966, the steel bridge is a multi-girder type. The span of interest is eighty-five feet. The exterior girders for this span are W36x230 members. Attached to the bottom of the girders are 0.875 inch cover plates. The fatigue strength of the cover plated girders with flange thickness greater than 0.800 inches have the lowest AASHTO fatigue rating, category E'. Since the flange thickness for a W36x230 is 1.260 inches, the AASHTO fatigue category is E'. The average girder spacing is 7.58 feet. The concrete deck acts as a composite. There is a 2 inch haunch. Fig. 3.2 presents a schematic of the steel girder and cover plate.

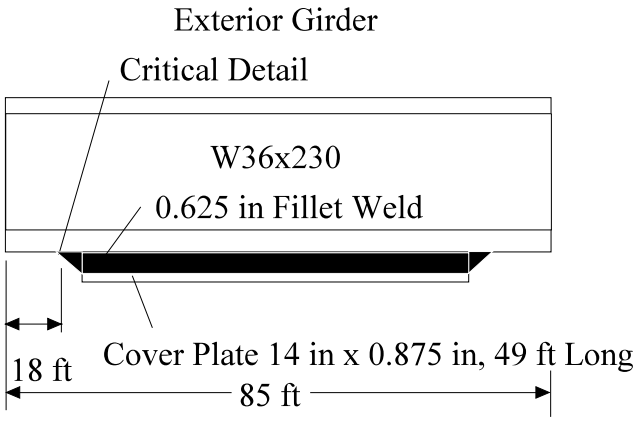

Fig. 3.2 Welded Cover Plate Girder, Detail No. 3

3.2.1 AASHTO Guide Specifications

The following is the evaluation of the remaining fatigue life using the AASHTO *Guide Specifications*:

1) S_{FL} equals 0.9 ksi, from section 3.3.

2) The nominal stress range at the detail is:

$$S_r = \frac{(M_{live} \cdot DF) \cdot y}{I} \qquad (2.5)$$

The impact factor is 1.10 for smooth pavement conditions in accordance with section 2.4. The maximum negative live load moment equals zero, since the span is simply supported. The maximum positive live load moment at the detail, 18 feet from the left support, occurs when the fatigue truck is placed according to Fig. 3.3.

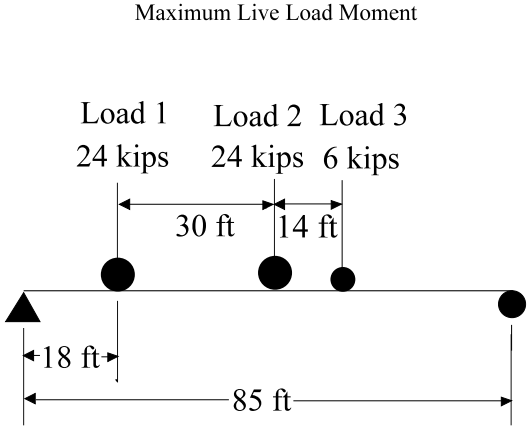

Fig. 3.3 Location of Fatigue Truck Resulting in Maximum Live Load Moment for Detail No. 3

The maximum positive moment including impact is found to be 612 k-ft.

The distribution factor for one lane is $DF_e = S/D$. S equals 7.58 feet, girder spacing, and D

= 21.7 (interpolation from the table in section 2.6). Then, $DF_e = 0.349 < (S - 3)/S = 0.604$.

According to the AASHTO *Specifications*, section 10.38.3.1, the effective flange width of the concrete is the girder spacing which is 6.21 feet. Using the transformed section shown in Fig. 3.4, the distance y between the neutral axis and the detail is found to be 30.1 inches. The total moment of inertia is $I_T = 34{,}300$ in^4

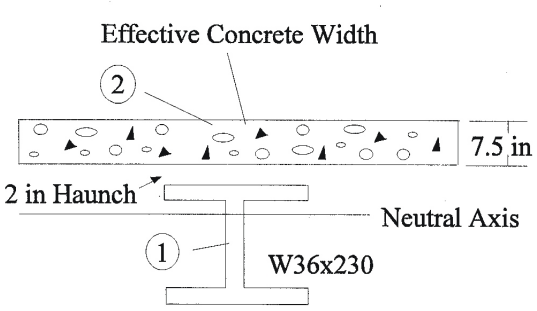

Fig. 3.4 Composite Concrete Bridge Deck, Detail No. 3

Including a factor of 1.15 from section 2.7.1 for a composite deck,

$$S_r = \frac{(612 \cdot 12 \cdot 0.349) \cdot 30.1}{34{,}300} \cdot \frac{1}{1.15}$$

$$S_r = 1.96 \text{ ksi}$$

3) $$R_S = R_{S0} \cdot F_{S1} \cdot F_{S2} \cdot F_{S3} = 1.35 \qquad (2.6)$$

$R_{S0} = 1.35$ This is a redundant member.
$F_{S1} = 1.0$ No measurements.
$F_{S2} = 1.0$ Standard fatigue truck used.
$F_{S3} = 1.0$ Normal procedure used.

4) $1.35 \cdot S_r > 0.9$ Therefore, the fatigue life is finite.

5) Remaining safe fatigue life,

$$Y_f = \frac{f \cdot K \times 10^6}{T_a \cdot C \cdot (R_S \cdot S_r)^3} - a \qquad (2.7)$$

f = 1.0 safe life
K = 1.1 from table in section 3.3
T_a = 1.02·2193 = 2240
1.02 comes from figure 3.5A, where the annual growth rate, g, is 0.7 percent
2193 = $ADT \cdot F_T \cdot F_L$
ADT = 17,200 from traffic data
F_T = 0.15 fraction of trucks
F_L = 0.85 fraction of trucks in outer lane, see table in section 3.5.
Number of lanes = 2, 1-way traffic.
C = 1.0 cycles per truck passage. See section 3.4 for longitudinal members part (a) simple span girders 40 feet or more
a = 28 years, present age of bridge

$$Y_f = \frac{1.0 \cdot 1.1 \times 10^6}{2240 \cdot 1.0 \cdot (1.35 \cdot 1.96)^3} - 28$$

Y_f = -1.5 remaining safe fatigue years

Remaining mean fatigue life,

$$Y_f = \frac{f \cdot K \times 10^6}{T_a \cdot C \cdot (R_S \cdot S_r)^3} - a \qquad (2.7)$$

f = 2.0
R_S = 1.0
All other factors are the same as the remaining safe fatigue life calculation.

$$Y_f = \frac{2.0 \cdot 1.1 \times 10^6}{2240 \cdot 1.0 \cdot (1.0 \cdot 1.96)^3} - 28$$

Y_f = 103 remaining mean fatigue years

3.2.2 LEFM

The remaining fatigue life is now calculated for detail No. 3 using LEFM. Since detail No. 3 is a welded cover plate end, values for a_i and a_{cr} are the same as in detail No. 1. The same correction factor equations (2.32-2.35) are again used as in detail No. 1. However, for a W36x230, the flange width, $2 \cdot b$, is 16.470 inches and the flange thickness, t_f, is 1.260 inches. The cover plate has a thickness, t_c, of 0.875 inch, and the weld leg size, Z, can be estimated from the maximum and minimum weld sizes as 0.625 inch (Blodgett 1968).

The total fatigue life in cycles, N, of this detail can be determined from:

$$N = \frac{1}{2.05 \cdot 10^{-10}} \int_{a_i}^{a_{cr}} \frac{1}{(F_s \cdot F_w \cdot F_g \cdot F_e \cdot S_r \cdot \sqrt{\pi \cdot a})^{3.0}} da \qquad (2.30)$$

S_r equals 1.96 ksi. This is the nominal stress range as calculated previously using the AASHTO *Guide Specifications*. Having defined all of the variables in the above integration, the total fatigue life in cycles is,

N = 43,900,000 cycles

Now that the total fatigue life in cycles has been determined, the remaining fatigue life in years will be determined using the BAR7 approach.

GF_1 = 0.05 past growth factor

n = 1994 - 1966 = 28 years

$ADTT_{1994}$ = 2193

Knowing the GF_1, n, and $ADTT_{1994}$, the $ADTT$ for 1966 can be determined from equation (2.18). From this, the accumulated number of cycles can be calculated from equation (2.10),

$$M = 365\frac{days}{year}\cdot[ADTT_{1966}]\cdot\frac{(1+GF_1)^n-1}{GF_1} \qquad (2.10)$$

M = 11,900,000 accumulated cycles

Knowing the $ADTT_{1994}$, N, M, and the future growth factor, GF_2, the remaining fatigue life in years, R, can be evaluated.

GF_2 = 0.01 future growth factor

$$R = \frac{\ln\left[\frac{(N-M)\cdot GF_2}{365\frac{days}{year}\cdot ADTT_{1994}\cdot(1+GF_2)}+1\right]}{\ln(1+GF_2)} \qquad (2.11)$$

R = 39.4 remaining years

Again, to demonstrated the validity of this procedure using LEFM a plot of the stress range versus the number of cycles is made using equation (2.30). This plot can then be compared to the AASHTO curve for fatigue category E', Fig. 2.8. These plots are quite similar as expected.

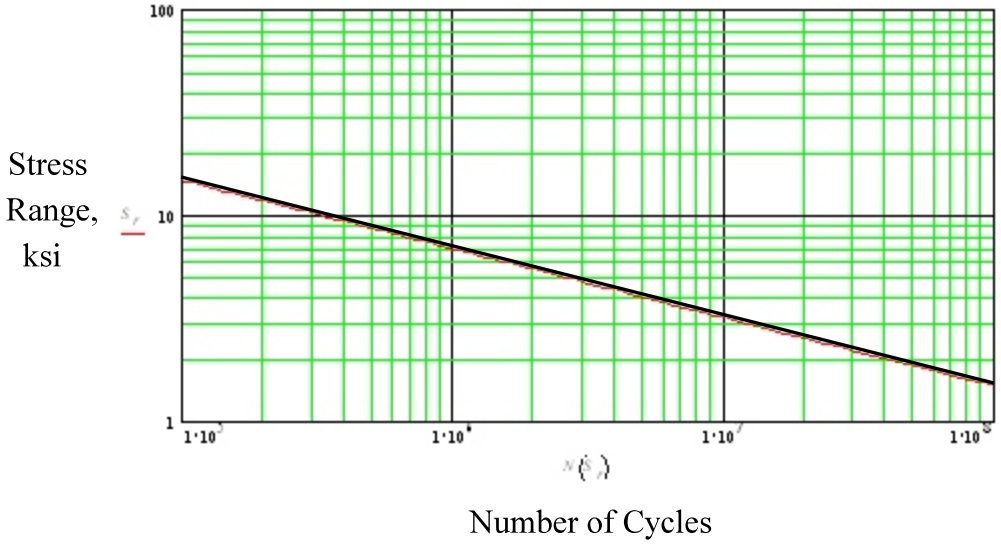

Fig. 3.5 Stress Range Versus Number of Cycles
using LEFM, Detail No. 3

3.3 Welded Cover Plate End, Detail No. 4

Bridge number 661 consists of three simple spans, and is located in Cranston, Rhode Island. Built in 1965, the steel bridge is a multi girder type. The center span is 77 feet. The interior girders for the center span are W36x150 members. Attached to the bottom of the girders are 1.25 inch cover plates. The fatigue strength of the cover plated girders with flange thickness greater than 0.8 inch have the lowest AASHTO fatigue rating, category E'. Since the flange thickness for a W36x150 is 0.940 inches, the AASHTO fatigue category is E'. The average girder spacing is 7 feet. The concrete deck acts as a composite. There is a 1 inch haunch. Fig. 3.6 presents a schematic of the steel girder and the cover plate.

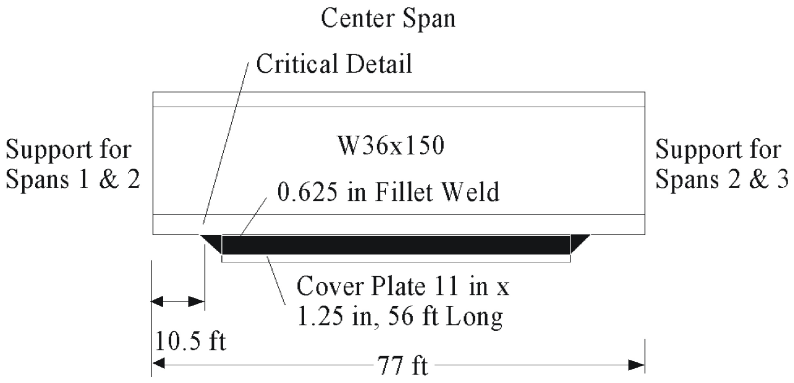

Fig. 3.6 Welded Cover Plate Girder, Detail No. 4

3.3.1 AASHTO Guide Specifications

The following is the evaluation of the remaining fatigue life using the AASHTO *Guide Specifications*:

1) S_{FL} equals 0.9 ksi, from section 3.3.

2) The nominal stress range at the detail is:

$$S_r = \frac{(M_{live} \cdot DF) \cdot y}{I} \qquad (2.5)$$

The impact factor is 1.10 for smooth pavement conditions in accordance with section 2.4. The maximum negative live load moment equals zero, since the span is simply supported. The

maximum positive live load moment at the detail, 10.5 feet from the left support, occurs when the fatigue truck is placed according to Fig. 3.7. Including the impact factor, it is 391 k-ft.

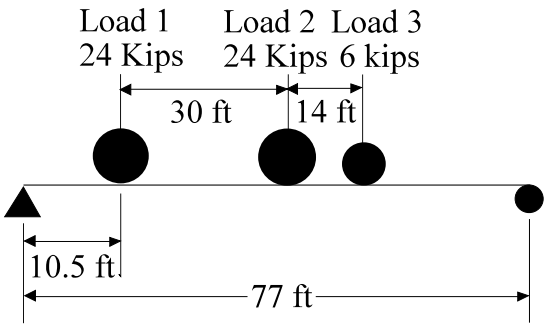

Fig. 3.7 Location of Fatigue Truck Resulting in Maximum Live Load Moment at Detail No. 4

The distribution factor for one lane is $DF_i = S/D$. S equals 7 feet, girder spacing and D=21.1 (section 2.6). Then, $DF_i = 0.33$ ($< (S - 3)/S = 0.57$).

Fig. 3.8 depicts a schematic of the transformed section. The effective flange width of the concrete is the girder spacing, 7 feet. The distance y between the neutral axis and the detail is found to be 31.9 inches, and the total moment of inertia is,

$$I_T = 23{,}300 \text{ in}^4$$

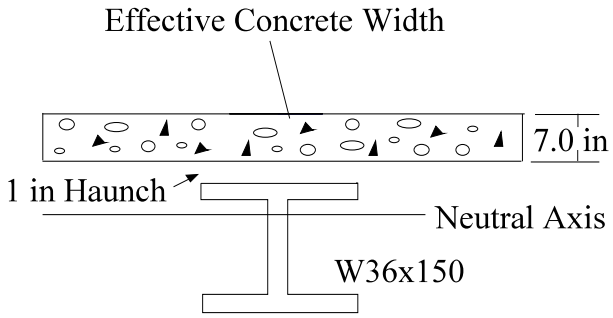

Fig. 3.8 Composite Concrete Bridge Deck, Detail No. 4

Including a factor of 1.15 from section 2.7.1 for the case of composite deck,

$$S_r = \frac{(391 \cdot 12 \cdot 0.33) \cdot 31.9}{23{,}300} \cdot \frac{1}{1.15}$$

$$S_r = 1.84 \text{ ksi}$$

3) $$R_S = R_{S0} \cdot F_{S1} \cdot F_{S2} \cdot F_{S3} \qquad (2.6)$$

$R_{S0} = 1.35$ This is a redundant member.
$F_{S1} = 1.0$ No measurements.
$F_{S2} = 1.0$ Standard fatigue truck used.
$F_{S3} = 1.0$ Normal procedure used.

$$R_S = 1.35$$

4) $1.35 \cdot S_r > 0.9$ Therefore, the fatigue life is finite.

5) Remaining safe fatigue life,

$$Y_f = \frac{f \cdot K \times 10^6}{T_a \cdot C \cdot (R_S \cdot S_r)^3} - a \qquad (2.7)$$

$f = 1.0$ safe life
$K = 1.1$ from table in section 3.3
$T_a = 1.04 \cdot 9211 = 9580$
1.04 comes from figure 3.5A, where the annual growth rate, g, is 2 percent
$9211 = ADT \cdot F_T \cdot F_L$
$ADT = 76{,}760$ (one-way average daily traffic)
$F_T = 0.15$ fraction of trucks
$F_L = 0.80$ fraction of trucks in outer lane, see table in section 3.5.
Number of lanes = 4, 1-way traffic.
$C = 1.0$ cycles per truck passage. See section 3.4 for longitudinal members part (a) simple span girders 40 feet or more
$a = 29$ years, present age of bridge

$$Y_f = \frac{1.0 \cdot 1.1 \times 10^6}{9580 \cdot 1.0 \cdot (1.35 \cdot 1.84)^3} - 29$$

Y_f = -21.5 remaining safe fatigue years

A negative number implies that there is no safe fatigue life remaining for this detail. The remaining mean fatigue life is determined by

$$Y_f = \frac{f \cdot K \times 10^6}{T_a \cdot C \cdot (R_S \cdot S_r)^3} - a \qquad (2.7)$$

f = 2.0
R_S = 1.0
All other factors are the same as the remaining safe fatigue life calculation.

$$Y_f = \frac{2.0 \cdot 1.1 \times 10^6}{9580 \cdot 1.0 \cdot (1.0 \cdot 1.84)^3} - 29$$

Y_f = 7.9 remaining mean fatigue years

3.3.2 LEFM

The remaining fatigue life is now calculated for detail No. 4 using LEFM. Since detail No. 4 is a welded cover plate end, values for a_i and a_{cr} are the same as in detail No. 1. The same correction factor equations (2.32-2.36) are again used as in detail No. 1. However, for a W36x150, the flange width, $2 \cdot b$, is 11.975 inches and the flange thickness, t_f, is 0.940 inch. The cover plate has a thickness, t_c, of 1.25 inch, and the weld leg size, Z, can be estimated from the maximum and minimum weld sizes as 0.625 inch (Blodgett 1968).

The total fatigue life in cycles, N, of this detail can be determined from:

$$N = \frac{1}{2.05 \cdot 10^{-10}} \int_{a_i}^{a_{cr}} \frac{1}{(F_s \cdot F_w \cdot F_g \cdot F_e \cdot S_r \cdot \sqrt{\pi \cdot a})^{3.0}} da \qquad (2.30)$$

S_r equals 1.84 ksi. This is the nominal stress range as calculated previously using the AASHTO *Guide Specifications*. Having defined all of the variables in the above integration, the total fatigue life in cycles is,

N = 70,500,000 cycles

Now that the total fatigue life in cycles has been determined, the remaining fatigue life in years will be determined using the BAR7 approach.

GF_1 = 0.05 past growth factor, n = 1994 - 1965 = 29 years

$ADTT_{1994}$ = 9211

Knowing the GF_1, n, and $ADTT_{1994}$, the $ADTT$ for 1965 can be determined from equation (2.18). From this, the accumulated number of cycles can be calculated from equation (2.10),

$$M = 365 \frac{days}{year} \cdot [ADTT_{1965}] \cdot \frac{(1 + GF_1)^n - 1}{GF_1} \qquad (2.10)$$

M = 50,900,000 accumulated cycles

Knowing the $ADTT_{1994}$, N, M, and the future growth factor, GF_2, the remaining fatigue life in years, R, can be evaluated.

GF_2 = 0.02 future growth factor

$$R = \frac{\ln\left[\dfrac{(N - M)\cdot GF_2}{365\dfrac{days}{year}\cdot ADTT_{1994}\cdot(1+GF_2)} + 1\right]}{\ln(1+GF_2)} \qquad (2.11)$$

R = 23.1 remaining years

Again, to demonstrate the validity of the LEFM procedure, a plot of the stress range versus the number of cycles is made using equation (2.30). This plot can then be compared to the AASHTO curve for fatigue category E', Fig. 2.8. These plots are quite similar as expected.

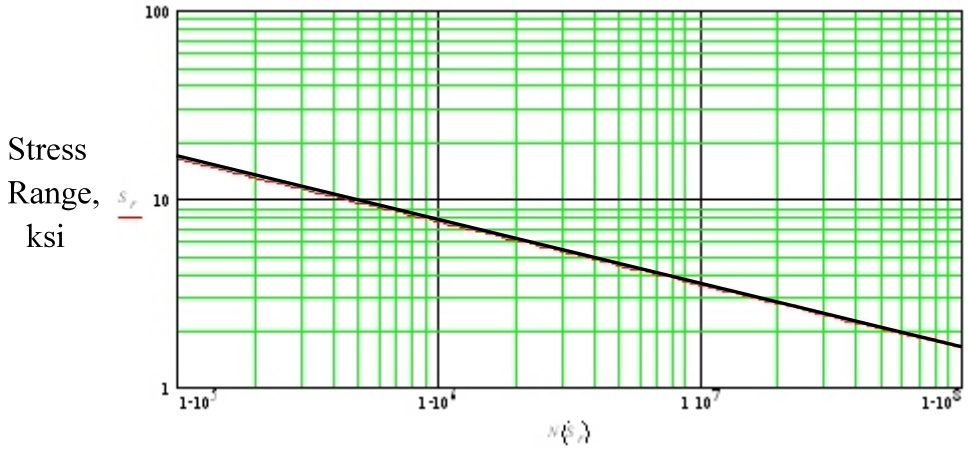

Number of Cycles

Fig. 3.9 Stress Range Versus Number of Cycles
Using LEFM, Detail No. 4

3.4 Welded Cover Plate End, Detail No. 5

Bridge number 525 is a multigirder bridge with eighteen spans. The structure is located on interstate 195 over the Providence River in Providence, Rhode Island. Span eight is 83 feet long. The bridge was built in 1958. The interior girders for this span are W36x280. Attached to the bottom of the girders are 0.625 inch cover plates. The fatigue strength of the cover plate girders with flange thickness greater than 0.800 inches has the lowest AASHTO fatigue rating, category E'. Since the flange thickness for a W36x280 is 1.570 inch, the AASHTO fatigue rating category is E'. The average girder spacing is 6.1 feet. The concrete deck has no composite action. There is no haunch. Fig. 3.10 shows a schematic of the steel girder and the cover plate.

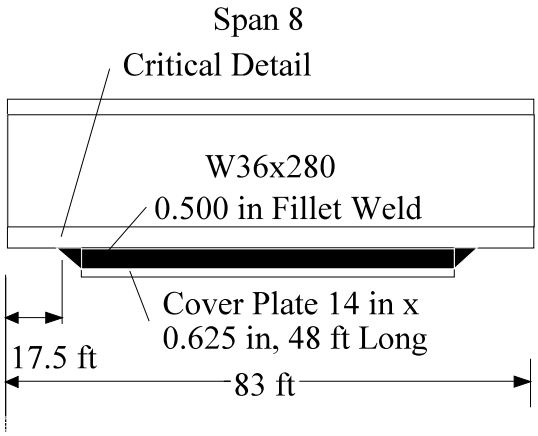

Fig. 3.10 Welded Cover Plate Girder, Detail No. 5

3.4.1 AASHTO Guide Specifications

The following is the evaluation of the remaining fatigue life using the AASHTO *Guide Specifications*:

1) S_{FL} equals 0.9 ksi, from section 3.3.

2) The nominal stress range at the detail is:

$$S_r = \frac{(M_{live} \cdot DF) \cdot y}{I} \qquad (2.5)$$

The impact factor is 1.24 for fairly rough pavement conditions in accordance with section 2.4. The maximum negative live load moment equals zero, since the span is simply supported. The maximum positive live load moment at midspan occurs when the fatigue truck is placed as shown in Fig. 3.11. Including the impact factor, it is 769 k-ft.

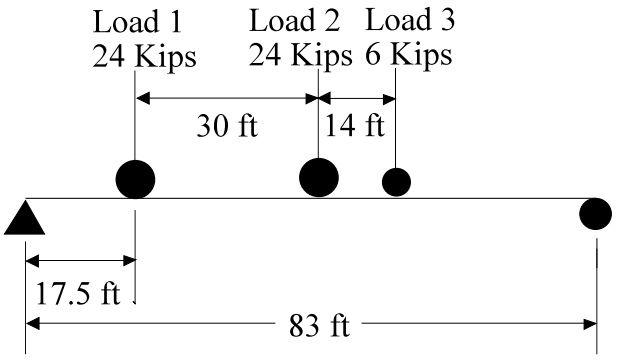

Fig. 3.11 Location of Fatigue Truck Resulting in Maximum Live Load Moment at Detail No. 5

The distribution factor for one lane is $DF_i = S/D$. The girder spacing S equals 6.1 ft, and D is 21.5 (section 2.6). The, DF_i = 0.284 (< (S - 3)/S = 0.508).

From Fig. 3.12, the distance y between the neutral axis and the detail is 18.3 inches. The

inertia of section 1 is, $I_T = 18{,}900$ in^4

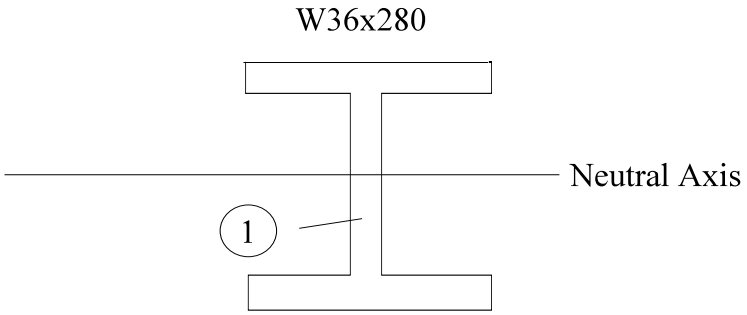

Fig. 3.12 Non-composite Concrete Bridge Deck, Detail No. 5

An additional factor of 1.30 is used since there is non-composite action of the bridge deck (section 2.7).

$$S_r = \frac{(769 \cdot 12 \cdot 0.284) \cdot 18.3}{18{,}900} \cdot \frac{1}{1.30}$$

$$S_r = 1.95 \text{ ksi}$$

3) $$R_S = R_{S0} \cdot F_{S1} \cdot F_{S2} \cdot F_{S3} \qquad (2.6)$$

$R_{S0} = 1.35$	This is a redundant member.
$F_{S1} = 1.0$	No measurements.
$F_{S2} = 1.0$	Standard fatigue truck used.
$F_{S3} = 1.0$	Normal procedure used.

$$R_S = 1.35$$

4) $1.35 \cdot S_r > 0.9$ Therefore, the fatigue life is finite.

5) Remaining safe fatigue life,

$$Y_f = \frac{f \cdot K \times 10^6}{T_a \cdot C \cdot (R_S \cdot S_r)^3} - a \qquad (2.7)$$

f = 1.0 safe life
K = 1.1 from table in section 3.3
T_a = 1.02·7500 = 7650
1.02 comes from figure 3.5A, where the annual growth rate, g, is 2 percent
7500 = $ADT \cdot F_T \cdot F_L$
ADT = 150,000 from traffic data
F_T = 0.10 fraction of trucks
F_L = 0.50 fraction of trucks in outer lane (approximated)
C = 1.0 cycles per truck passage. See section 3.4 for longitudinal members part (a) simple span girders 40 feet or more
a = 34 years, present age of bridge

$$Y_f = \frac{1.0 \cdot 1.1 \times 10^6}{7650 \cdot 1.0 \cdot (1.35 \cdot 1.95)^3} - 34$$

Y_f = -26.4 remaining safe fatigue years

The negative sign indicates that the safe fatigue life has expired. The mean fatigue life is:

$$Y_f = \frac{f \cdot K \times 10^6}{T_a \cdot C \cdot (R_S \cdot S_r)^3} - a \qquad (2.7)$$

f = 2.0
R_S = 1.0
All other factors are the same as the remaining safe fatigue life calculation.

$$Y_f = \frac{2.0 \cdot 1.1 \times 10^6}{7650 \cdot 1.0 \cdot (1.0 \cdot 1.95)^3} - 34$$

Y_f = 4.8 remaining mean fatigue years

3.4.2 LEFM

The remaining fatigue life is now calculated for detail No. 5 using LEFM. Since detail No. 5 is a welded cover plate end, values for a_i and a_{cr} are the same as in detail No. 1. The same correction factor equations (2.32-2.35) are again used as in detail No. 1. However, for a W36x280, the flange width, $b_f=(2\cdot b)$, is 16.595 inches and the flange thickness, t_f, is 1.570 inch. The cover plate has a thickness, t_c, of 0.625 inch, and the weld leg size, Z, can be estimated from the maximum and minimum weld sizes as 0.500 inch (Blodgett 1968).

The total fatigue life in cycles, N, of this detail can be determined from the following equation,

$$N = \frac{1}{2.05\cdot 10^{-10}} \int_{a_i}^{a_{cr}} \frac{1}{(F_s \cdot F_w \cdot F_g \cdot F_e \cdot S_r \cdot \sqrt{\pi \cdot a})^{3.0}} da \qquad (2.30)$$

S_r equals 1.95 ksi which is the nominal stress range as calculated previously using the AASHTO *Guide Specifications*. Having defined all of the variables in the above integration, the total fatigue life in cycles is,

$$N = 28{,}000{,}000 \text{ cycles}$$

Now that the total fatigue life in cycles has been determined, the remaining fatigue life in years can be determined using the BAR7 approach.

$$GF_1 = 0.09 \text{ past growth factor, } n = 1992 - 1958 = 34 \text{ years}$$

$$ADTT_{1992} = 7650$$

Knowing the GF_1, n, and $ADTT_{1992}$, the $ADTT$ for 1958 can be determined from equation (2.18).

From this, the accumulated number of cycles can be calculated from equation (2.10),

$$M = 365\frac{days}{year}\cdot[ADTT_{1958}]\cdot\frac{(1+GF_1)^n-1}{GF_1} \qquad (2.10)$$

M = 29,400,000 accumulated cycles

Knowing the $ADTT_{1992}$, N, M, and the future growth factor, GF_2=0.01, the remaining fatigue life is:

$$R = \frac{\ln\left[\frac{(N-M)\cdot GF_2}{365\frac{days}{year}\cdot ADTT_{1992}\cdot(1+GF_2)}+1\right]}{\ln(1+GF_2)} \qquad (2.11)$$

R = -2.1 remaining years

Again, to demonstrate the validity of this procedure using LEFM, a plot of the stress range versus the number of cycles is made using equation (2.30). This plot can be compared to the AASHTO curve for fatigue category E', Fig. 2.8. These plots are quite similar as expected.

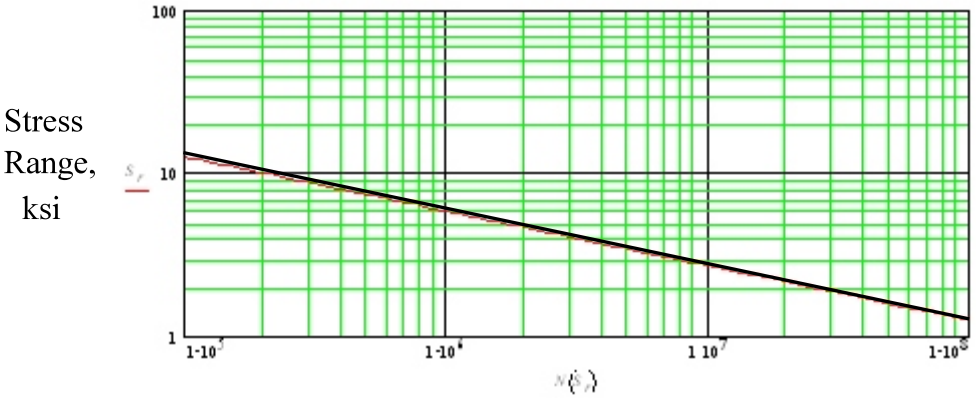

Fig. 3.13 Stress Range Versus Number of Cycles Using LEFM, Detail No. 5

4.0 ANALYSIS OF RESULTS

4.1 Fatigue Life Comparisons

Five fatigue prone details have been examined using the AASHTO Guide Specifications and LEFM, three in chapter 3 and two in chapter 2. Table 4.1 summarizes some pertinent information of the bridge details considered such as stress range, ADTT, and the calculated total fatigue life of the bridges. The remaining fatigue life of the bridges can be found by subtracting the age of the bridge from the total fatigue life. Following the AASHTO approach, both the safe and the mean fatigue lives are listed. Four of the details have finite fatigue lives which is typical of welded cover plate end details with AASHTO fatigue category E′. The other detail, a welded web connection with AASHTO category C, has infinite fatigue life. This is reasonable considering that stresses in the web are less than stresses occurring at the flange bottom.

Of the four welded cover plate ends, the nominal stress range, S_r, based on the fatigue truck, varies from 1.74 to 1.96 ksi which is a narrow range. Two details have *ADTT* volumes of 2000 and 2240 which represent moderate truck traffic, while the other details have much higher volumes of 9580 and 7650. These differences in *ADTT* account for a majority of the variations in the calculated fatigue lives.

All members are redundant so the safe fatigue life corresponds to 97.7 percent probability that the actual fatigue life will exceed the calculated life. The mean fatigue life corresponds to a 50 percent probability of exceedance and it is the most likely probabilistic estimate of the actual fatigue life given this methodology as well as the manner in which the parameters are determined.

Detail No.	Age (years)	Composite Deck	Type of Detail	S_r (ksi)	*ADTT*	Method		
						LEFM	AASHTO *Guide Specifications*	
							Safe	Mean
1	34	Y	Welded Cover Plate End	1.74	2000	74.6	42.5	209.0
2	29	Y	Welded Web Connection	0.68	1320	251.0	∞	∞
3	28	Y	Welded Cover Plate End	1.96	2240	67.4	26.5	131.0
4	29	Y	Welded Cover Plate End	1.84	9580	52.1	7.5	36.9
5	34	N	Welded Cover Plate End	1.95	7650	31.9	7.9	38.8

*All the above details have redundant members. Detail No. 2 has an AASHTO fatigue category of C whereas all the others have AASHTO fatigue category of E'.

Table 4.1 Total Fatigue Life (in years)

The difference between the total safe life and total mean life may appear unusually large, but these differences are typical. This can be explained by examining both total safe fatigue life and total mean fatigue life. According to the NCHRP 299 from which the current AASHTO *Guide Specifications* on fatigue are based, the ratio of mean to allowable stress range averages 1.243. This includes fatigue categories B through E'. The average ratio of total mean fatigue life to total safe fatigue life can be calculated as shown in NCHRP 299 as,

$$R_{m\text{-}s} = (R_S \cdot 1.243)^3 \tag{5.1}$$

For redundant members, $R_S = 1.35$. Therefore,

$$R_{m\text{-}s} = (1.35 \cdot 1.243)^3 = 4.7 \approx 5$$

For nonredundant members, this ratio is approximately 10.

Thus, for the typical detail with a redundant member, if the total safe fatigue life is calculated to be 20 years, the total mean fatigue life is 100 years. The factor of 5 applies to the ratio of the total mean fatigue life to the total safe fatigue life for details with redundant members. The ratio of the remaining mean fatigue life to the remaining safe fatigue life may be significantly higher than this. For example, in detail No. 1 the remaining safe fatigue life is 8.5 years and the remaining mean fatigue life is 175 years. In this case, the ratio of the remaining mean fatigue life to the remaining safe fatigue life is approximately 20.

Table 4.1 also includes fatigue life predictions using the LEFM. In this case, the stress range is the most important parameter. The *ADTT* is also important in determining the accumulated cycles.

All four welded cover plate ends using LEFM result in fatigue lives significantly longer than the safe fatigue life, Table 4.1. Neither the AASHTO *Guide Specifications* nor the LEFM are exact. In each, there are parameters with large uncertainties. In the AASHTO *Guide Specifications*, these

are the stress range, *ADTT*, and the traffic (truck) growth rates. In LEFM, these are the initial and critical crack sizes as well as the ones mentioned for the AASHTO *Guide Specifications*.

"Fatigue is a principle failure mode for steel structures, and it is less understood than any other modes of failure." (Zhao, Haldar, and Breen 1994). Despite this, reasonable approximations have been made using these methods.

4.2 Current Practice

When should a detail be considered for inspection, monitoring, rehabilitation or even possible replacement purposes? Should this be based on the remaining safe fatigue life, the remaining mean fatigue life, or based on LEFM, or some other criteria? Current practice uses the remaining safe fatigue life because of the inherent conservatism.

According to the AASHTO *Guide Specifications* for a detail not meeting the required remaining safe fatigue life, the engineer must follow certain options such as: calculating the remaining safe fatigue life more accurately, restricting traffic on the bridge, repairing the bridge, or establishing periodic inspections. Low remaining safe fatigue life values usually prompt the engineer to make a site specific evaluation.

Typically, engineers do not consider the remaining mean fatigue life. An examination of many current fatigue reports from six different engineering companies indicates that only one of them calculated the remaining mean fatigue life in addition to the remaining safe fatigue life.

For example, a fatigue analysis was performed on an interior girder of a bridge's center span. The girder consisted of a welded cover plate end, and the member was redundant. The remaining safe fatigue life was calculated by the engineer to be -9.6 years. The remaining mean fatigue life was

not calculated. If calculated, it would have been 69.8 years. Following the AASHTO *Guide Specifications*, the engineer had two options. Option one was to retrofit the welded cover plate ends with bolt splices. Option two was to perform periodic inspections to assure adequate safety without any changes in the detail. Since a recent field inspection by an engineering consulting company found no fatigue cracks, the engineer recommended option two. While the engineer made the right decision given the circumstances, the whole process raises questions as to the appropriateness of the remaining safe fatigue life as the controlling fatigue criteria.

Fatigue evaluations are only performed 2 to 3 times during the life of a steel bridge corresponding to major rehabilitation work. For that reason, engineers often recommend one of the previously mentioned options even when the remaining safe fatigue life is high, for example 40 years.

4.3 Comments on Fatigue Evaluations

The purpose of a fatigue evaluation is to identify and quantify the fatigue potential of a steel highway bridge. While it is impossible to determine the precise amount of remaining fatigue life, reasonable estimates can be determined. With these estimates, cost effective decisions can be made including categorizing of bridges for future inspection and testing purposes.

Welded longitudinal stiffener and transverse stiffener ends, Fig. 4.1, of very old bridges with deep girders and thin webs, as well as welded cover plate ends of bridges built during the 1950's, 60's, and early 1970's need to be considered for fatigue evaluation. Of the three above mentioned details, welded cover plate ends are the most frequently encountered in Rhode Island.

From the preceding discussion it is obvious that safe fatigue life calculations tend to be conservative. For non-redundant bridges such conservatism is warranted. For non-redundant cases a less conservative procedure is proposed in Chapter 5. According to that method a coefficient is introduced in the standard AASHTO Guide Specifications in order to determine the so-called practical remaining fatigue life of a bridge detail.

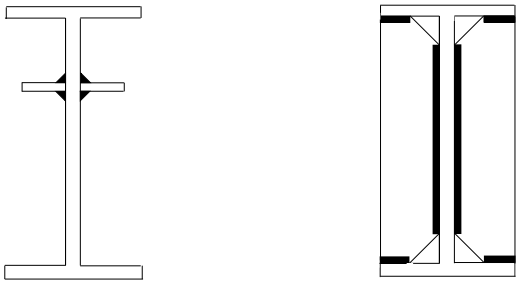

a) b)

Fig. 4.1 Girder Attachments: a) Longitudinal Stiffener, and b) Transverse Stiffener

5.0 RECOMMENDED FATIGUE CRITERIA

5.1 Introduction

Table 5.1 at the end of this chapter, summarizes the remaining fatigue life of the four cover-plated examples considered. The LEFM fatigue life is substantially longer than the safe fatigue life of the AASHTO guide specifications. Current practice uses the remaining safe fatigue life as recommended by the AASHTO guide specifications as the governing fatigue criteria. Since the remaining safe fatigue life is often only calculated corresponding to major rehabilitation projects, remaining safe fatigue life values of 30 years or less are often assumed as nearing the end of the fatigue life thereby prompting the engineer to consider retrofitting or replacement.

Bridge 3 on Table 5.1 is a simple span bridge built in 1966 in Richmond, RI, Fig. 5.1. A low remaining safe fatigue life of -1.5 years prompted a complete retrofit of the cover plate ends. Every detail of this type on the bridge was bolt spliced, Fig. 5.2. Was this retrofit appropriate given that the remaining mean fatigue life and LEFM estimates are 103 and 39.4 years, respectively?

For the case of nonredundant bridges the conservatism associated with the use of the safe remaining fatigue life is needed but for the case of redundant bridges the criteria could be relaxed. Most of the research involved with the development of the fatigue specifications concentrated on the strength part of the problem. Current research on the loading component may lead to improved predictions and a more narrow margin between the mean and the safe fatigue life estimates. In the meantime, an adjustment factor is developed here which can be introduced in the fatigue life equation for the case of bridge details with redundant members and produce closer agreement with the fracture mechanics based estimates for the four bridges considered.

Fig. 5.1 Bridge in Richmond, RI

Fig. 5.2 End Cover-Plate Rehabilitation

5.2 Recommended Fatigue Criteria for Redundant Bridges

The total fatigue life according to AASHTO *Guide Specifications* is,

$$Y_f = \frac{f \cdot K \times 10^6}{T_a \cdot C \cdot (R_S \cdot S_r)^3} \tag{2.7}$$

where terms are defined earlier, in Chapter 2. The fatigue life factor, *f*, is 1.0 or 2.0 depending on whether the safe or mean fatigue life is desired. The safe and mean fatigue life expressions for details with redundant members resulting from equation (2.7) are respectively,

$$Y_f = \frac{1.0 \cdot K \times 10^6}{T_a \cdot C \cdot (1.35 \cdot S_r)^3} \tag{5.1}$$

$$Y_f = \frac{2.0 \cdot K \times 10^6}{T_a \cdot C \cdot (1.0 \cdot S_r)^3} \tag{5.2}$$

The proposed fatigue life expression for details with redundant members considers modifying Eq. 5.2 by multiplying the total mean fatigue life by a factor, R_f, (Tsiatas and Palmquist, 1999). This is termed the redundancy factor, R_f, so as not to be confused with any other variable in the AASHTO *Guide Specifications* procedure. The resulting expression is,

$$Y_f = R_f \cdot \frac{2.0 \cdot K \times 10^6}{T_a \cdot C \cdot (1.0 \cdot S_r)^3} \tag{5.3}$$

Since the mean fatigue life represents a 50 percent exceedance probability, the redundancy factor should remain less than 1.0 to remain conservative. It is noted that a value of R_f=0.2 corresponds to the safe fatigue life whereas a value of R_f=1 corresponds to the mean fatigue life. It is not the

intent here to establish appropriate levels of safety but to demonstrate that various probability levels can be achieved using the form of Eq. 5.3. In the case of the four example bridges a value of R_f=0.5 is arbitrarily selected for better agreement with the fracture mechanics results. This corresponds to a probability of 85% that the actual fatigue life will exceed the calculated fatigue life of the bridge. This probability can be determined by realizing that Eq. 5.3 can be looked at as the safe fatigue life, Eq. 5.1, where the reliability factor R_S equals 1.0 instead of 1.35 for redundant members. From figure 15 of the NCHRP 299 where R_S is γ, the safety index, β, corresponds to approximately 1.0. Using a complementary standard normal table with safety index, β equal to 1.0, the nominal failure probability, Φ(-β), is 0.15 (Melchers 1987). The probability that the actual fatigue life will exceed the predicted life is 1 - Φ(-β) or 85 percent. Fig. 5.3 provides a graph of the redundancy factor versus the probability that the actual fatigue life will exceed the calculated fatigue life.

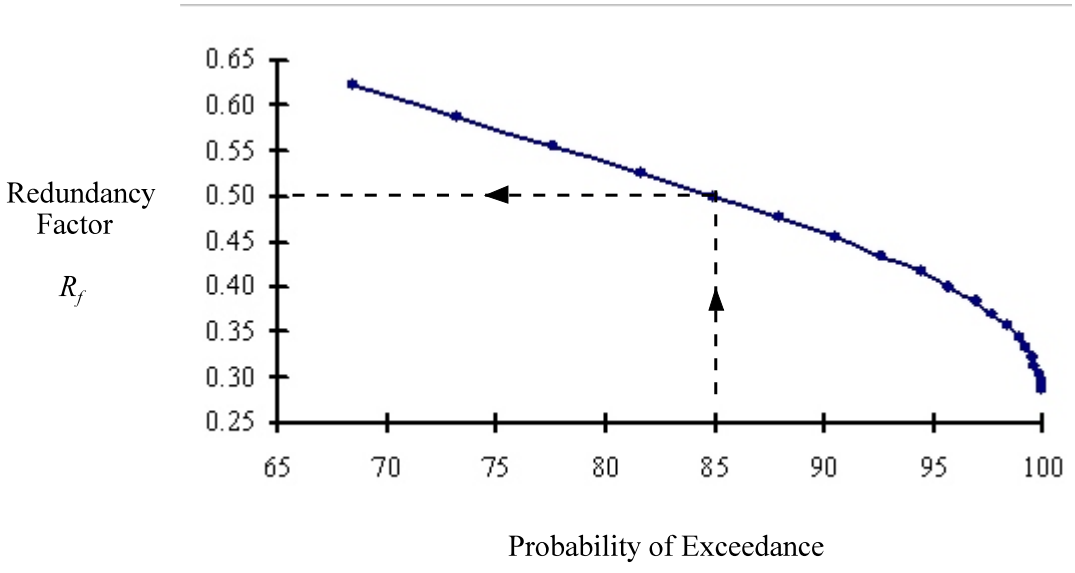

Figure 5.3 Redundancy Factor Versus Probability of Exceedance

The resulting expression for the fatigue life is still conservative like the safe fatigue life.

Although this is not as highly conservative, this level of safety is more rational and practical. The redundancy factor, R_f, can be modified to reflect future research and trends just like many of the variables in the AASHTO *Guide Specifications*. Substituting 0.5 into equation (5.3) for R_f,

$$Y_f = 0.5 \cdot \frac{2.0 \cdot K \times 10^6}{T_a \cdot C \cdot (1.0 \cdot S_r)^3} \tag{5.4}$$

Further simplification of this expression results in the following,

$$Y_f = \frac{K \times 10^6}{T_a \cdot C \cdot S_r^3} \tag{5.5}$$

The remaining practical fatigue life is found by subtracting the current age of the bridge as:

$$Y_f = \frac{K \times 10^6}{T_a \cdot C \cdot S_r^3} - a \tag{5.6}$$

Eq. 5.6 providing the remaining practical fatigue life accounts for better agreement with LEFM results. Table 5.2 summarizes the safe, mean, practical and LEFM total and remaining fatigue lives for the four bridge details considered. Considering that the remaining safe fatigue life has been exhausted for three of the above four welded cover plate ends, a remedial decision under current AASHTO *Guide Specifications* would have to be made since. Even the welded cover plate detail with a remaining safe fatigue life of 8.5 years should according to the AASHTO *Guide Specifications* have its remaining safe life recalculated using an improved method. Using the remaining practical fatigue life, only two of the four details need to be further investigated for fatigue

crack potential at this time.

The benefits of using the remaining practical fatigue life over the remaining safe fatigue life for redundant members are significant. Limits on safety are set at reasonable levels which may be modified in the future. Finally, more justifiable, cost effective decisions can be made including categorizing bridges for future inspection and testing purposes.

Bridge	**Safe**		**Mean**		**Practical**		**LEFM**	
	total	remaining	total	remaining	total	remaining	total	remaining
1	42.5	8.5	209	175	104.4	70.4	74.6	40.6
3	26.5	-1.5	131	103	65.3	37.3	67.4	39.4
4	7.5	-21.5	36.9	7.9	18.4	-10.6	52.1	23.1
5	7.9	-26.1	38.8	4.8	19.4	-14.6	31.9	-2.1

Table 5.1 Total and Remaining Fatigue Life of the Cover-Plated Bridge Details

6.0 FATIGUE TESTING

6.1 Overview

Fatigue, fracture and loss of section due to corrosion are the three characteristics of steel bridges that have the potential to damage their integrity. In the present study we concentrate on evaluating the fatigue life but for existing and deteriorated bridges the other two factors may be important.

During the design stage one can only make reasonable assumptions on the amount and weight of truck loads on the bridge. Also, material properties and structural configuration are known. The same is not true for existing and deteriorated bridges. Design formulae can allow for an approximate and hopefully conservative estimate of the remaining fatigue life of the bridge but for an accurate assessment field testing would be needed.

Fatigue testing is the process of measuring and monitoring stresses at a particular detail as well as determining the fatigue life experimentally. With this and information on the type and nature of the detail as well as the material type, fatigue resistance can be evaluated. Details are examined individually. From a practical point of view, only fatigue prone details having an AASHTO fatigue category of D, E, and E' need to be considered. These categories contain details that have been known to fracture in actual steel bridges. Specific types of details found to be particularly susceptible to fatigue include cover plates and large plate-type attachments to tension flanges of girders, ends of certain fillet-welded connections, longitudinal stiffeners on girder webs, plug welds and slot welds, and cruciform welds (Hahin et. al. 1993).

There are two issues in fatigue studies of steel bridges, detection of cracks and fatigue life estimate. Many methods based on advanced technologies have been developed for crack detection.

These tend to be expensive and localized. Usually, they will only be applied in cases that there is a high confidence of crack existence. Some of the methods include:

- Thermographic imaging. This is based on the use of high resolution thermographic imaging systems to detect surface-breaking cracks. The method uses active heating of the bridge surface with a high-wattage light to detect cracks. A special pattern of hot and cold regions is created on the surface and an image of heat flow patterns is obtained. Cracks are detected by characteristic heat flow patterns The system has detected fatigue cracks covered by paint.
- Acoustic Emission. Several studies have been made on using acoustic emission technology to detect crack initiation and study the crack propagation. It all centers on changing acoustic properties emitted from an appropriately instrumented bridge.
- Ultrasonics. This is one of the most commonly used crack detection techniques in steel structures. A sound beam is induced in the material being inspected and reflections of that beam are interpreted to determine the location and size of cracks.
- Eddy Current Detection. This technique uses induced magnetic fields to inspect the surface of conductive materials such as steel.
- NUMAC. This is a New Ultrasonic and Magnetic Analyzer for Cracks that combines ultrasonic and magnetic inspection methods into a single crack detection instrument.

These methods would be used for QA/QC purposes or in case of high probability of cracks. Typically, fatigue testing relates to methodology to evaluate the remaining fatigue life of a bridge and not necessarily to detect a specific crack.

6.2 Field Testing for Improved Fatigue Life Estimate of Rhode Island Bridges

Field strain monitoring is the appropriate procedure for an accurate determination of the fatigue life of existing and deteriorated bridges. There are usually two procedures used to determine the remaining fatigue life of existing bridges, both relying on measurements of strains.

The first, traditional, approach includes monitoring of the strains at critical bridge locations over a certain time period. The period is chosen so that continuous and representative traffic induced strains are collected. At a minimum a 24 hour period is needed but if traffic patterns vary seasonally, such monitoring would have to be repeated several times a year. The strain or deduced stress time history is analyzed following the "rainflow" method to determine an approximate count of straining cycles that the particular bridge detail has been exposed to. An histogram of stress frequencies is developed for the monitored period and by extrapolation for the time since bridge construction. This is used in conjunction with established SN curves to estimate damage and remaining life.

In the present study the method based in the AASHTO Guide Specifications is recommended for the evaluation of the remaining fatigue life of the bridges. This approach provides the remaining fatigue life as

$$Y_f = \frac{f \cdot K \times 10^6}{T_a \cdot C \cdot (R_S \cdot S_r)^3} - a \qquad (2.7)$$

The various constants in this equations were described earlier in chapter 2. For an improved fatigue life estimate more accurate estimate of these coefficients is warranted. Note that K is a detail constant relating the susceptibility of the particular detail to fatigue damage. It depends on the fatigue category of the detail. Since we are not advocating to introduce new details this is provided

in the literature. In case of new steels or different details additional testing would have to be undertaken similar with the tests at Lehigh University which formed the basis for the fatigue-prone details. The factor *f* is the safe or mean or perhaps "practical" fatigue life factor. This depends on the safety limits assumed in the specification. The factors that can be improved by field monitoring are R_s, T_a, C, and S_r.

6.2.1 Stress Range, S_r

This is one of the most important factors affecting fatigue life. Typically, it is calculated analytically using the code specified fatigue truck and analyzing a mathematical model of the bridge. The model can be simple, based on beam theory, or complex using finite elements. However, for an existing and deteriorated bridge this mathematical model does not necessarily describe accurately the bridge condition. For example, bridge elements may be deteriorated, support conditions can be far from ideal and bearings may have deteriorated to a point that mathematical assumptions would not reflect the true condition. As a result of such uncertainty, engineers develop conservative models and carry out conservative analytical procedures. The result can be a very conservative estimate of the stress range. It is also possible that a significant defect may have escaped detection and the resulting stress estimate to be unconservative.

Field monitoring to determine the stress range based on a stress-range histogram obtained from field measurements under normal traffic is the single most important way to improve fatigue estimates of the bridge.

6.2.2 Number of Stress Cycles per Truck Passage, *C*

For very short span bridges the passage of the fatigue truck causes two distinct stress cycles, one for each truck axle. For longer span bridges, the passage of the fatigue truck causes a complex cycle which can be analyzed to determine an equivalent number of individual cycles. In determining the coefficient C in AASHTO Guide Specifications a table was prepared of number of cycles per truck passage for different span lengths. However, this is an aggregate of many observations and one would expect to be conservative for any individual bridge.

Trucks crossing a bridge, in addition to large stress cycles associated with the movement of static loads, cause vibrations. These are usually small and were neglected in the determination of the factor C. There may be cases however, that due to the structural system at hand or the condition of the deteriorated bridge that these vibrations may be significant. Hence, for an accurate fatigue life estimate of an existing and deteriorated bridge an accurate determination of the number of cycles C per truck passage is important.

The number of cycles C can be determined from the stress history of the bridge obtained through field monitoring. NCHRP Report 299 provides a procedure similar to the "rainflow" approach to determine the equivalent number of simple cycles for a complex stress time history.

6.2.3 Reliability Factor, R_s

The reliability factor, R_S, is given by the following expression:

$$R_S = R_{S0} \cdot F_{S1} \cdot F_{S2} \cdot F_{S3} \qquad (2.6)$$

where R_{S0} is the basic reliability factor which equals to 1.35 for redundant members and 1.75 for nonredundant members. F_{S1}, F_{S2}, and F_{S3} are procedure factors which account for the stress range,

gross weight of fatigue truck, and lateral distribution, respectively.

The AASHTO Guide Specifications set a target safety or reliability index β to 2.0 for redundant and 3.0 for nonredundant bridge members. For the case of redundant members this corresponds to a probability 97.7% that the actual fatigue life will exceed the calculated one. This probability increases to 99.9% for the case of non-redundant bridge members. Based on these reliability levels the basic reliability factor R_{so} equals to 1.35 for redundant members and 1.75 for nonredundant ones. Factors F_{s1}, F_{s2}, and F_{s3} are used to modify the basic reliability factor depending with the increased accuracy of the data and calculations. They are equal to one if standard procedures, data and calculations are used. Different values are suggested in cases of better information.

Factor Fs_1 depends on the procedure used for the calculation of the stresses. When the standard procedure with the fatigue truck is used, this factor is one. But, when stress ranges are determined from field monitoring, less variability is present and the coefficient is reduced to 0.85. Since this coefficient affects the denominator of the equation and is raised to a power of 3, the effect on fatigue life estimates can be significant.

Factor F_{s2}, relates to site truck weight data. Assuming more precise information on truck weight distribution this coefficient could be reduced although NCHRP Report 299 suggests that the difference would be relatively small. In case that gross weight histograms could be developed using weigh-in-motion measurements, the coefficient could be reduced to 0.95. Factor Fs_3 corresponds to the lateral distribution factor used. A detailed study such as field measurement would allow for a modest reduction to 0.96.

6.2.4 Lifetime Average Daily Truck Volume, T_a

T_a represents the lifetime average daily truck volume in the outer lane. This is determined from the present truck volume in the outer lane and the use of assumed truck-volume growth rates. A factor F_L is applied to the ADT at the site to account for the percentage of trucks in the traffic and the percentage of trucks in the shoulder lane. The Guide provides typical percentages of trucks in traffic as well as the factor F_L. However, because of the importance of this coefficient for fatigue life calculations it is suggested that traffic data need to be available and processed to obtain these values.

6.3 Field Monitoring

From the previous discussion it is obvious that field monitoring of stresses and traffic are very important for accurate fatigue life estimates. This is especially true for existing, deteriorated bridges where actual bridge conditions are not known and stress calculations can be very approximate. The direct benefit of field monitoring would be an accurate estimate of the parameter S_r, the parameter C, as well as a reduction in the coefficient Fs_1 from 1 to 0.85.

Although what is actually used in fatigue calculations is the stress range, strains are typically monitored and these are used to calculate stresses. The traditional approach for strain monitoring in steel bridges is the use of electrical resistance strain gauges. These would need to be installed near critical details. Collected data could be stored locally and retrieved manually but for an efficient monitoring program some automated system would need to be employed for remote data collection.

Fiber optic based strain sensors have recently been employed for monitoring various parameters including strain in bridges. This is an active area of research for development of robust

systems to be employed in the field. Low cost promises to bring such sensors to the forefront of data collection. A novel fiberoptic sensor for displacement monitoring was studied by one of the co-PIs of this project and the related report is included as Appendix A.

One of the problems of a field strain monitoring is the need to install gauges at various locations on the bridge, and connect them with wires to a central location where a remote data collection system can be located. Continuous power is also needed at this central location. Recently, FHWA sponsored the development of a wireless strain measurement system which consists of rugged, battery-powered, radio transponder modules. These can accept up to four standard resistive strain gauges with all power and signal conditioning provided by the transponder. Up to 10 of these transponders can be used simultaneously. This system is still under development with cost and battery life the limiting factors.

Other technologies are under development for bridge strain/stress monitoring including a measurement system that uses electromagnetic acoustic transducers and a so-called passive fatigue load monitoring devices which monitors the propagation of a crack in a pre-cracked coupon.

Considering the state of the technology, a strain gauge based system is recommended for immediate deployment to monitor bridge strains with a simultaneous investment in research on laboratory and field prototype studies of fiber optic based sensors.

6.4 Prioritizing Bridges for Fatigue Evaluation

In Rhode Island, the vast majority of bridges consist of single simply supported or multiple simply supported spans. Many of these bridges are considered structurally deficient. Fig. 6.1 shows the percentage of structurally and functionally Rhode Island deficient bridges in the NHS.

To properly address the problem of fatigue, bridges with details known to have low fatigue life should be examined first. The most common fatigue prone details encountered in Rhode Island bridges are welded cover plate ends. These details were used to increase the moment of inertia of the girder while keeping the depth constant. Another detail that is rather rare, is a longitudinal stiffener weld which may appear in much older bridges and was used to avoid web buckling.

In the present study, a listing of bridges with cover plate details was obtained. These were prioritized according to the average daily traffic ADT, as well as the condition of the superstructure. The condition of the superstructure is rated from 1 to 8 (1 meaning excessive deterioration and 8 meaning brand new). The following is a list of bridges arranged by interstate with fatigue priority rating. Only bridges with known cover plates are ranked in sequential order. A ranking of 1 corresponds to the worst possible fatigue ranking. It should be noted that this listing may need updating with new information. Also, it reflects information available to investigators in1996.

Of particular importance are bridges with rating 1 through 10. These bridges have high volumes of traffic. High volumes of *ADT* are encountered on I-95 and I-195. Only moderate volumes of *ADT* occur on I-295.

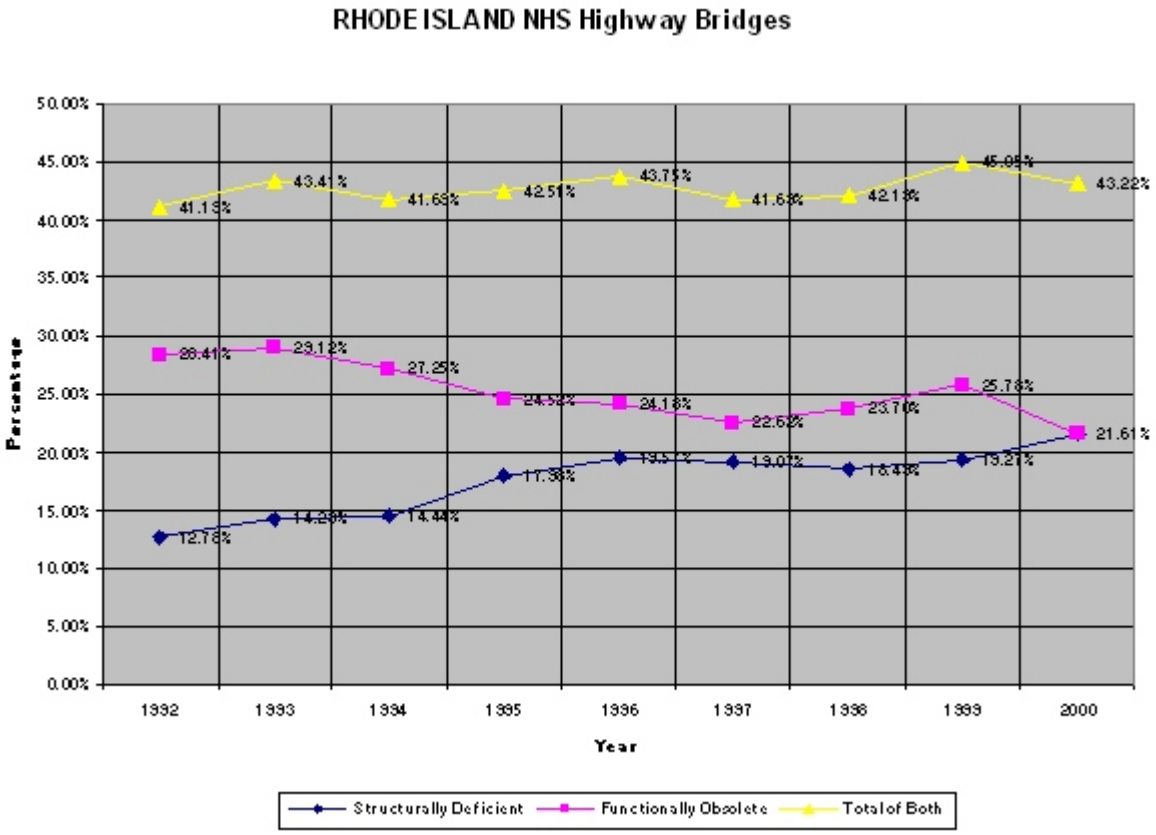

Fig. 6.1 Rhode Island NHS Deficient Bridges

ROUTE I-95

BIN No.	Facility Carried	Feature Intersected	Total Spans	Year Built	Superstruc. Condition	Cover Plate	ADT	Priority Rating
051801	I-95 ND & SB	RI 2 Quaker Lane	2	1958	5	Y	109800	9
053201	Lane C	I-95, I-195 Int Com	3	1963	6	Y	38700	14
053701	I-95 & Ramps	Eddy St	1	1961	5	Y	162200	1
055001	I-95	Taft St & Seeknk Rr	5	1958	5	Unk	111000	-
055101	I-95 & Ramp	Elm St	1	1958	6	Unk	111600	-
055201	I-95	Water St	3	1958	6	Unk	111000	-
055401	I-95	School St	1	1958	4	Unk	95000	-
056101	I-95 NB	East St	3	1964	6	Y	35000	16
056121	I-95 SB	East St	3	1964	5	Y	35000	15
056201	I-95 NB	Roosevelt Av	3	1964	6	Y	32700	19
056221	I-95 SB	Roosevelt Av	3	1964	6	Y	32700	20
056301	I-95 NB	Amtrk & Plea VW St	5	1964	6	Y	32800	17
056321	I-95 SB	Amtrk & Plea VW St	5	1964	6	Y	32800	18
057801	I-95	US6, Woon Rr, Amt	8	1964	5	Unk	170000	-
058601	I-95 NB	Weaver Hill Rd	1	1968	7	Y	15600	27
058621	I-95 SB	Weaver Hill Rd	1	1968	7	Y	15600	28
059101	I-95 NB	Ten Rod Rd	1	1968	6	Y	14400	32
059121	I-95 SB	Ten Rod Rd	1	1968	6	Y	14700	31
059301	I-95	Relocated Rte 3	1	1969	4	Y	28600	22
065501	I-95	Thurbers Av	2	1963	6	Y	155000	6
065901	I-95	US 1 Elmwood Av	3	1965	4	Unk	155000	-
066001	I-95	Amtrak	4	1964	6	Y	155000	7
066101	I-95	Wellington Av	3	1964	5	Y	162200	2
068301	I-95	Toll Gate Rd	1	1965	4	Y	109800	8
068401	I-95	RI 117 Centrvlle Rd	2	1965	8	Y	109800	10
068601	I-95	S County Fwy Ramp	1	1965	7	Y	54900	13
070601	I-95	Amtrak & P&W Rr	1	1963	5	Y	160000	3
070701	I-95	Ashburton St	1	1963	5	Y	160000	4
070801	I-95	Charles St	1	1963	6	Y	160000	5

ROUTE I-195

BIN No.	Facility Carried	Feature Intersected	Total Spans	Year Built	Superstruc. Condition	Cover Plate	ADT	Priority Rating
020001	I-195 EB	Seeknk Rr, Rr & Sts	15	1930	4	N	55000	-
052201	I-195	Bridge St & Sr-2	3	1958	6	Unk	154500	-
052501	I-195	Providence Rr	18	1958	5	Unk	154500	-
052801	I-195 Cr-4	Dyer St	3	1957	5	Unk	9000	-
052901	I-195	Richmond St	1	1957	5	Unk	154500	-
053001	I-195	Chestnut St & Sr-12	3	1957	4	Unk	154500	-
053101	I-95, I-195 INIR C	Lane J	1	1963	6	Y	60000	11
070001	I-195 WB	Seekonk Rr	18	1969	4	Y	55000	12

ROUTE I-295

BIN No.	Facility Carried	Feature Intersected	Total Spans	Year Built	Superstruc. Condition	Cover Plate	ADT	Priority Rating
071901	I-295 NB	I-95 SB	3	1966	5	Y	28000	24
072201	I-295 NB	RI 2 Bald Hill Rd	2	1967	4	N	28000	-
072221	I-295 SB	RI 2 Bald Hill Rd	2	1967	6	N	28000	-
072501	I-295 NB	Wash Sc Rr; W N Rd	4	1968	4	Y	14800	29
072521	I-295 SB	Wash Sc Rr; W N Rd	4	1968	6	Y	14800	30
073001	I-295 NB	Water Supply Aquad	3	1968	5	N	22100	-
073021	I-295 SB	Water Supply Aquad	3	1968	5	N	22100	-
073201	I-295 NB	RI 14 Plainfld Pke Av	1	1969	7	N	22100	-
073221	I-295 SB	RI 14 Plainfld Pke Av	1	1969	4	N	22100	-
073601	I-295 NB	Ramp 6	1	1971	5	Y	28900	21
073621	I-295 SB	Ramp E-N	1	1971	5	Y	28500	23
073701	I-295 NB	US 6	2	1971	6	N	28100	-
073721	I-295 SB	US 6	2	1971	6	N	28100	-
074001	I-295 NB	RI 5 Greenville Av	1	1970	5	N	22400	-
074021	I-295 SB	RI 5 Greenville Av	1	1970	5	N	22400	-
074501	I-295 NB	Stillwater Rd	1	1970	5	Y	11800	39
074521	I-295 SB	Stillwater Rd	1	1970	6	Y	11800	40
074801	I-295 NB	RI 146 Eddie D Hwy	2	1969	6	N	13400	-
074821	I-295 SB	RI 146 Eddie D Hwy	2	1969	6	N	13400	-
075001	I-295 NB	Blckstn Rr & P&W Rr	4	1964	6	N	13500	-
075021	I-295 SB	Blckstn Rr & P&W Rr	4	1964	6	N	13500	-
075201	I-295 NB	Scott Rd	3	1965	6	Y	13000	33
075221	I-295 SB	Scott Rd	3	1965	6	Y	13000	34
075301	I-295 NB	Leigh Rd	3	1965	7	Y	13000	35
075321	I-295 SB	Leigh Rd	3	1965	7	Y	13000	36
075501	I-295 NB	Abbott Run Valley Rd	3	1965	6	Y	12700	37
075521	I-295 SB	Abbott Run Valley Rd	3	1965	7	Y	12700	38
075701	I-295 NB	Hartford Pike	2	1971	6	Y	22900	25
075721	I-295 SB	US 6 Hartford Pike	2	1971	6	Y	22900	26

7.0 CONCLUSIONS AND RECOMMENDATIONS

The state of practice for fatigue evaluation has been an evolutionary process originating with design and testing. From this, theories evolved such as Miner's law. This law sparked many methods of fatigue prediction including the AASHTO *Guide Specifications*, BAR7, and the Lehigh method. Other theories of damaged accumulation also evolved such as the LEFM.

Presently, the AASHTO *Guide Specifications* is primarily used for all fatigue evaluations of existing steel bridges. It is important to remember that fatigue evaluations are not precise nor accurate. Calculating the remaining fatigue life provides an estimate only. Uncertainty is due to the lack or inability to obtain the nominal stress range at a detail as well as predicting future traffic flow and fatigue life at a detail. Using the AASHTO *Guide Specifications* with site specific data will improve fatigue life predictions significantly. Evaluations based on site specific data are more accurate than standardized procedures such as the use of the fatigue truck to determine the nominal stress range.

For this project, four methods of fatigue evaluations have been examined. They are the AASHTO *Guide Specifications*, BAR7, the Lehigh method, and LEFM. These methods are used to determine the remaining fatigue life of two bridge details, a cover plate and a welded web connection.

Results from these two examples demonstrate that fatigue predictions made using the AASHTO *Guide Specifications* and LEFM are more accurate than the other two methods. Three more cover plate ends from actual steel highway bridges are examined using the AASHTO *Guide Specifications* and LEFM since welded cover plate ends represent the majority of fatigue related problems in Rhode Island.

The study revealed large differences between the remaining safe fatigue life and the remaining mean fatigue life as well as predictions made using a fracture mechanics-based procedure. Current practice relies primarily on the remaining safe fatigue life as the governing criterion which is more conservative than the remaining mean fatigue life. However, it may result in premature monitoring and expenses. For the case of steel bridges with redundant members an adjustment factor is introduced and a "practical" fatigue life is calculated. Using various values of this factor different probability levels can be achieved. For a value of 0.2 the practical and the safe fatigue coincide. A value of 0.5 produces fatigue estimates which are in better agreement with fracture mechanics-based estimation for four bridges.

The importance of field monitoring for accurate fatigue life predictions is stressed. Various potential monitoring systems are listed. It is recommended that bridges are instrumented with strain gauges for strain monitoring at fatigue critical details. Analysis of the time histories will allow to accurately determine the stress range, as well as other factors needed for an accurate estimate of the remaining fatigue life of the bridge. This is important because modeling assumptions will give poor analytical results for existing and deteriorated bridges. It is also suggested that research is undertaken to develop a fiber-optic system for bridge strain monitoring.

It is difficult to develop a priority listing of bridges for fatigue evaluation. An approximate list was developed based on Average Daily Traffic, and superstructure condition for cover plated bridges in the major highways.

REFERENCES

AASHTO., *Guide Specifications for Fatigue Evaluation of Existing Steel Bridges*, Interim 1993, Washington, D. C., 1990.

Albrecht, P., and N. Yazdani. "Risk Analysis Extending the Service Life of the Steel Bridges," *Report FHWA/MD No. 84/01*, 1986.

Barsom, J. M., and S. T. Rolfe. "Fracture and Fatigue Control in Structures: Applications of Fracture Mechanics." Englewood Cliffs, N.J., Prentice-Hall, 1987.

Blodgett, O. W., "Design of Welded Structures." James F. Lincoln Arc Welding Foundation, Cleveland, OH 1968.

Breon, J. A., and M. L. Hasmukh. "User's Manual for Computer Program Bridge Analysis and Rating (BAR7)", Pennsylvania Department of Transportation, 1991.

Chase, S. B. "NDE for Steel Bridges." ASCE (May 1995), 49-51.

Collacott, R. A., "Structural Integrity Monitoring," New York, N.Y. Chapman and Hall, 1985.

Fisher, J. W., and M. A. Hirt., "Fatigue Crack Growth in Welded Beams." *Engineering Fracture Mechanics*, 1973.

Fisher, J. W; Hausammann, H.; Sullivan, M.; and A. Pense. "Detection and Repair of Fatigue Damage in Welded Highway Bridges," *NCHRP Report 206*, Transportation Research Board, Washington D. C., 1979.

Fisher, J. W., "Fatigue and Fracture in Steel Bridges: Case Studies," John Wiley & Sons, New York, 1984.

Fisher, J. W.; Yen, B. T.; and D. Wang. "Fatigue Cracking of Steel Bridge Structures," *Report*

FHWA No. RD-89-168, 1989.

Hahin, C. et. al. "Accurate and Rapid Determination of Fatigue Damage in Steel Bridges." Journal of Structural Engineering, January 1993, pp. 150-167.

Hertzberg, Richard W., "Deformation and Fracture Mechanics of Engineering Materials." John Wiley and Sons, New York, 1989.

Keating, Peter B. "Focusing of Fatigue." *ASCE*, November 1994, pp. 54-57.

Laman, Jeffrey A., and A. S. Nowak., "Fatigue-Load Models for Girder Bridges." *Journal of Structural Engineering*, July 1996, pp. 726-733.

Melchers, R. E., "Structural Reliability: Analysis and Prediction."John Wiley & Sons, New York, 1987.

Moses, F., and William E. Nyman. "Load Simulation for Bridge Design and Life Prediction," Report, Case Western Reserve University, Department of Civil Engineering, Cleveland, OH, 1984.

Moses, F.; Snyder, R. E.; and G. E. Likins, "Loading Spectrum Experienced by Bridge Structures in the United States," *Report FHWA/RD-85/012*, Bridge Weighing Systems, Warrenville, OH, 1985.

Moses, F.; Schilling, C. G.; and K. S. Raju, "Fatigue Evaluation Procedures for Steel Bridges," *NCHRP Report 299*, Transportation Research Board, Washington, D.C., 1987.

Shilling, C. G. et. al., "Fatigue of Welded Steel Bridge Members Under Variable-Amplitude Loadings," *NCHRP Report 188*, Transportation Research Board, Washington, D.C., 1978.

Tsiatas, G. And Palmquist, S., 1999. "Fatigue Evaluation of Highway Bridges," Probabilistic

Engineering Mechanics, Vol. 14, pp. 189-194.

Zhao, Z.; Haldar, A.; and F. L. Breen Jr., "Fatigue-Reliability Evaluation of Steel Bridges." *Journal of Structural Engineering*, May 1994, pp. 1608-623.

Zuraski, P. D., "Service Performance of Steel Bridges Compared to Fatigue-Life Predictions." *Journal of Structural Engineering*, October 1993, pp. 3057-67.

APPENDIX A

Report to the Rhode Island Department of Transportation
June 1996

Development of a Simple Fiber Optic Sensor for Health Monitoring of Bridge Structures

Frank Sienkiewicz and Arun Shukla
Dynamic Photomechanics Laboratory
Department of Mechanical Engineering and Applied Mechanics
University of Rhode Island
Kingston, RI 02881

Abstract

An intensity based fiber optic displacement sensor has been developed and tested for static and dynamic response. The sensor incorporates an extremely simple design, light source, and detector. Testing was done using quasi-static extension, a simple oscillating cantilever beam, and a small shaker capable of frequencies up to 10 kHz. The sensor shows response over a wide range of 410 mm. The response has two distinct linear regions with a central non linear region. For small displacements, the sensor shows excellent frequency response up to 10 kHz.

Key words: *fiber optics, displacement sensor, intensity based sensor, sensor sensitivity, sensor range, sensor accuracy, sensor frequency response.*

1 Introduction

Fiber optic sensors have long been touted for their potential application to 'smart structures applications. With the development of smart materials several off shoot technologies have also evolved. In particular, the use of optical fibers as sensors for the measurement of mechanical quantities has seen considerable growth. Most of these sensors are still intricate in their construction and require elaborate electronics. This paper presents a rather simple design for a displacement transducer with a large operating range.

A sampling of the benefits of fiber optic sensors over their conventional counterparts include their resistance to electromagnetic interference, resistance to hostile environments, light weight and small size. Also, an extensive array of ancillary components and systems have been developed by the communications industry and are available at relatively low cost. These many benefits are being exploited more and more for modern sensor design. Several studies using fiber optics for sensor design have appeared in recent years. A complete review of all of these is beyond the scope of this document but the following will serve to demonstrate the depth of the field of fiber optics as sensing elements.

One of the first demonstrations of the potential for optical fibers to be used as sensors was published in 1978[1]. Butter and Hocker[1] showed that optical fibers could be configured as a Mach-Zehnder interferometer and strain applied to one arm of the arrangement would result in a spatial shift of the interference pattern. This shift of the interference fringes was directly related to the applied strain. After this demonstration, many different groups and laboratories have accelerated the progress[2,3,4,5,6].

Applications of fiber optic sensors cover many diverse fields and needs. Commercial systems are currently available to measure process flow, flow pressure and levels, as well as strain, carbon dioxide and other gases, and there is also a system available that was designed to monitor temperatures in mines[7]. In recent years fiber optic sensors have gained considerable interest from the engineering community with the greatest interest lying in the development of 'smart materials'[8,9]. Their inherent geometry also makes them ideal for embedding in modern composite structures and applications exist for non destructive testing[10,11].

Fiber optic sensors have also found many applications in structural civil engineering problems[12]. One area for potential application of fiber optic sensors is health monitoring of civil structures. The proposed sensor is designed with this application in mind.

2 Types of Sensors

Fiber optic sensors can be categorized into one of two groups: intrinsic sensors, where the fiber itself is the sensing element, or extrinsic sensors, where an external element interacts with the light. In these two groups there are many ways in which the quantity to be measured may affect the light propagating in the fiber but the two most common types of interaction are phase modulation and intensity modulation.

Phase modulation relies on a retardation of some portion of the signal that when recombined with the original signal produces an optical interference pattern. The degree of retardation is then directly related to the quantity to be measured. Sensors of this type include the Mach-Zehnder, the Fabry-Perot, and the polarimetric sensor to name a few.

Intensity modulation based sensors can be as simple as an on/off type device where the signal is either disrupted or restored by the desired measurand, or more complex where a continuous monitoring can be achieved. The simple on/off devices, as their name implies, utilize a window or gate that is placed in the optical path which is controlled by the measurand. These sensors act in a threshold fashion where the desired parameter is not resolved discretely but rather a signal is generated when a preset level is reached. Intensity based devices that are capable of discrete monitoring are typically microbend type sensors. In both cases, however, the output intensity is monitored and the intensity modulation is related directly to the measurand.

First attempts at intensity based microbend sensors typically involved external deformer plates which caused microbends in the fiber. Recently researchers have demonstrated that microbends can be permanently introduced into the fiber[13], or selected etching of the fiber cladding[14] results in stress concentrations that will reduce the effective light carrying capability of the fiber. In both of these cases the researchers have nearly eliminated hysterisis problems inherent in sensors that utilize an external means to cause microbends.

3 Sensor Design

The sensor presented in this paper utilizes a continuous piece of multimode optical fiber (Corning 85/125) 'tied' into the shape of a figure of eight. A sketch of the sensor is shown in figure 1. The geometry allows the natural stiffness of the fiber to act as a restoring force which holds the shape of the sensor during extension and compression. Put simply, the fiber will attempt to 'unwrap' itself and return to a straight line were it not for the constraint imposed by the knot geometry. This sensor functions as an intensity based optical fiber strain or displacement transducer when it is bonded to a body at two points, one on each side of the loops. Since multimode fiber is used in the construction, a simple LED/PIN diode can be used for the light source and detector. Figure 2 shows a schematic of the setup for the sensor with the associated electronics for light source and detection.

As the two fixed points are displaced with respect to each other, the radii of curvature of the sensor loops changes. A tensile strain (extension) would result in a shrinking of the sensor loops and drop in light intensity measured at the detector. Conversely, a compressive strain would result in an expansion of the loops and an intensity increase at the detector.

The light source was a Motorola MFOE1200 diode coupled to a driving circuit utilizing a 10V DC supply. The detector was a Motorola MFOD1100 (matching component for the diode) with an 18V DC bias, which was coupled to a twenty times amplifier with a variable DC offset. The amplifier was powered with ±12V DC supply.

4 Experiments, Results, and Discussion

To investigate the range of the sensor an experiment was performed on an Instron testing machine using a sensor with an initial dimension of 150 mm (see figure 1) measured from one end of the loops to the other. The cross head on the testing machine was then extended at a slow speed (12.7 mm/min) while the sensor output was captured on a Nicolet digital storage oscilloscope. The

complete plot of sensor output versus extension is shown in figure 3 with the experimental points shown as symbols. Due to the large number of data points, only every 50th data point has been shown. The figure shows three distinct regions; a linear region with shallow negative slope, a nonlinear region, and a second linear region with a large negative slope. Each of these regions have been curve fit with equations. It should be noted that the plot is actually a composite of two separate runs. During the experiment the signal change exceeded the capabilities of the amplifier circuit so the test was stopped and the DC offset was utilized to shift the output level. The amount of the shift was then accounted for when compiling the data into the plot shown.

In the first linear region (0-200 mm), a least squares, first order curve fit was applied. A multiple correlation coefficient squared value, $R^2 = 0.957$, was obtained. Similar treatment was given to the third region (380-410 mm) with an $R^2 = 0.996$. The mean deviation from linearity in these regions was found to be 1.2 and 0.02 percent for the first and second regions, respectively. The maximum deviations from linearity were found to be 7.1 percent for the former and 8.4 percent for the latter region.

The central nonlinear region was fit with a hyperbolic expression of the form given in equation (1)

$$y = \frac{a\,x}{b + x}. \qquad \textbf{(1)}$$

Equation (1) represents a rectangular hyperbola where the curve rises asymptotically from 0 to a. The constant b represents the value of x at which the function y has reached 0.5a. Comparing this description of the behavior of the curve described by equation (1) to the graph shown in figure 3, it should be obvious that some manipulation of the expression is required before it can be utilized to fit the experimental data.

The first step is to solve equation (1) for x in order that the curve may be mirrored about the y axis by multiplying the resultant expression by negative one. Additionally, the curve must be shifted by some constant values in both the x and y directions (constants c and d, respectively, below). The new expression for x is given as

$$x = -\frac{(y + d)b}{a - (y + d)} + c \,. \tag{2}$$

Lastly, solving equation (2) for y and combining constants yields

$$y = \frac{e + fx}{g - x} \,, \tag{3}$$

where linear combinations of a, b, c, and d have been incorporated into the new constants e, f, and g for brevity.

A Marquardt-Levenberg algorithm was used to determine the parameters which minimize the least squares of the sum of differences between the dependant variables and the observed values. The result for the three curve fitting operations is a set of three functions which depend upon the extension from the original sensor size of 150 mm

$$f(x) = \begin{cases} y = m_1 x + b_1 & 0 \le x \le 200 \\ y = \dfrac{ex + f}{g - x} & 200 < x \le 380 \\ y = m_2 x + b_2 & 380 < x < 410 \end{cases} \,, \tag{4}$$

corresponding to the three regions described earlier. An important note is that figure (3) represents a complete calibration plot for the sensor. However, as the extension from the original size is a somewhat impractical reference, a relationship between sensor size and extension was sought.

Another experiment was conducted in which the sensor was extended over approximately

375 mm. The initial sensor size was set to 150 mm and extension was begun. Sensor dimension was measured at discrete points during the extension and the resulting plot is shown in figure 4. The figure shows a linear relationship between sensor size and extension which allows a direct transformation between the two through another first order least squares curve fit.

The data of figure 3 was used to evaluate the sensitivity of the sensor. Figure 5 shows the sensitivity, defined as the change in output per unit input, as a function of sensor dimension. The linear relationship derived from figure 4 transforms sensor extension to sensor size. The sensitivity is defined as the derivative of the output with respect to the input which in this case is done for the three separate functions of equation (4). Figure (5) better illustrates the various sensitivity regions and the fact that the sensitivity is directly related to the size of the sensor. As the sensor size decreases, the loop radii also decreases causing more light to be lost for a given input and thus increasing sensitivity.

Using the parameters obtained from the curve fitting of figure 3 and the derivatives of the functions defined in equation (4), the sensitivities were determined for the three regions. As stated, the smaller the sensor dimension, the higher the sensitivity. In its most sensitive configuration, (8-12 mm loop-to-loop dimension) the calibration constant was found to be approximately 475 mV/mm. Referring back to figure (3), the linear range at the highest sensitivity corresponds to the region of maximum extension (380-410 mm). So according to the data presented, the sensor has a sensitivity of 475 mV/mm over a range of approximately 30 mm at the highest sensitivity level. The second linear region shows a lower sensitivity but has a broader range. Namely, the sensitivity is approximately 8 mV/mm over a range of 200 mm. The nonlinear region represents a continuously changing sensitivity over approximately 160 mm.

Sensor repeatability was investigated by bonding one side of four sensors to a fixed point and the other side to a translation stage. The sensor were connected individually to the light source

and the detector and displaced through a 3 mm range. Output was monitored for each sensor and figure 6 shows a plot of the sensor output as a function of displacement. The plot shows good repeatability in construction and performance.

The sensor was then bonded to a cantilever beam opposite an electrical resistance strain gage as shown in figure 7. The beam was displaced and allowed to vibrate freely while both the strain gage output and the optical fiber sensor output were captured on an oscilloscope. The fiber sensor output was zero shifted and linearly scaled to fit the strain gage data with the result being shown in figure 8. The figure shows that the fiber optic sensor matched the electrical resistance strain gage quite well and showed no hysterisis. The match is so good that the two signals are virtually indistinguishable from each other and, consequently, only every 10th data point is plotted for the fiber sensor. The reader should not be mislead into thinking that the peak values from the fiber sensor do not correspond to those of the strain gage as this is only an artifact of the plotting scheme. In fact, the mean of the error between the strain gage signal and the fiber optic sensor was found to be less than 1 percent. This experiment also served as a low frequency response test (25 Hz) for the sensor.

Lastly, one side of the sensor was bonded to a fixed surface and the other end was attached to a Wilcoxon Research F4/F7 electromagnetic/piezoelectric shaker system. The system was driven by a Hewlett-Packard spectrum analyzer which was also used to collect data from both a built in accelerometer and the fiber optic sensor. The shaker was driven with a sinusoidal signal at 1,3,5,7 and 10 kHz. Figure 9 shows a portion of the time series for both the fiber optic sensor and the accelerometer subject to a frequency of 3 kHz. Fast Fourier transforms (FFT's produced automatically by the analyzer) for the 3 kHz run are shown in figure 10.The frequency plots show that the fiber optic sensor is in excellent agreement with the accelerometer with a much sharper peak in the fiber optic sensor data. It should also be noted that this data is for a single run with no

averaging which would tend to smooth the baseline noise in the data. All other tests produced similar results and the frequency plot for an oscillatory frequency of 10 kHz is shown in figure 11 for further comparison.

These frequency plots show excellent modal response from the sensor. However, the fiber optic sensor seems to suffer from a phase problem between 5-7 kHz. In this region the fiber optic sensor output shifts 180° in phase with respect to the accelerometer. Then at 10 kHz the fiber optic sensor flips 180° again. This phase shift shows no effect on the frequency resolution capabilities but it should be acknowledged that the time domain data would not be in agreement. So, while the sensor works quite well for frequency resolution, the data can not yet be reliably transformed into absolute displacements at higher frequencies.

5 Closure

A fiber optic sensor which is capable of low frequency displacement and high frequency modal analysis has been demonstrated. The sensor showed excellent agreement with conventional sensor technology. However, unlike conventional sensors, the fiber optic sensor provides virtually no reinforcing effects which may bias test results. The simple components and construction make it ideal for many applications where cost and ease of use may be factors. Low frequency displacements with two distinct linear ranges have been shown. Also high frequency response has been shown to 10 kHz.

Specifically, the sensor shows two distinctly linear regions with mean deviations from linearity of 1.2 and 0.02 percent. The maximum deviations from linearity in these regions was found to be 7.1 and 8.4 percent. One of the linear regions shows a sensitivity of 475 mV/mm over a 30 mm extension. The second region yields a broader range of 200 mm but a lower sensitivity, 8 mV/mm. When compared to existing strain gage technology on an oscillating cantilever beam, the sensor

showed a mean error within 1 percent.

Currently the sensor is being evaluated on a model bridge structure constructed in the laboratory. Figure 12 schematically represents the truss type structure. The fiber sensor has been bonded to various points on the structure along with an electrical resistance strain gage. Preliminary modal response results are shown in figure 13. The plot shows the fast Fourier transforms of the fiber optic sensor signal and the strain gage signal and represents the frequency characteristics of the bridge structure subject to dynamic shaker loading.

Acknowledgment

The authors would like to acknowledge the Air Force Office of Scientific Research under grant numbers F49620-93-1-0209 and F49620-93-1-0475 and the Rhode Island Department of Transportation.

References

1. Butter, C.D., and Hocker, G.B., (1978), "Fiber optics strain gauge", *Appl. Opt.* **17**, pp 2867-2869.

2. Sirkis, J., and Taylor C., (1988), "Interferometric-fiber-optic strain sensor", *Expt. Mech.*, **28**, pp. 170-176.

3. Lee, C., Taylor, H., Markus, A., and Udd, E., (1989), "Optical-fiber Fabry-Perot embedded sensor", *Opt. Lett.*, **14**, pp. 1225-1227, Nov. 1989.

4. Narendran, N., Shukla, A., and Letcher, S., (1991), "Determination of Fracture Parameters Using Embedded Fiber-optic Sensors," *Experimental Mechanics*, **4**, pp. 360-366.

5. Narendran, N., Shukla, A., and Letcher, S., (1992), "Optical-Fiber Interferometric Strain

Sensor Using a Single Fiber," *Experimental Techniques*, **16**(6), pp. 33-36.

6. Narendran, N., Letcher, S., and Shukla, A., (1993), "Optical-Fiber Strain Sensor Using Combined Interference and Polarization Technique," *Optics and Lasers in Engineering*, **18**, pp. 121-133.

7. Dubaniewicz, T.H., Chilton, J.E., and Dobroski, Jr., H., (1993), "Fiber Optics for Atmospheric Mine Monitoring," *IEEE Transactions on Industry Applications*, **29**(4), pp. 749-753.

8. Claus, R.,(1990), "Virginia Tech. Smart Structures Research Overview", *OE/Fibers '90*, San Jose, California, USA.

9. Measures, R., (1992), "Advances Toward Fiber Optic Based Smart Structures," *Optical Engineering*, **31**(1), pp. 34-47.

10. DePaula, R., Flax, L., Cole, J., and Bucaro, J., (1982), "Single-Mode Fiber Ultrasonic Sensor", *IEEE J. Quant. Elect.*, **QE-18**, pp 680-683.

11. Narendran, N., Zhou, C., Letcher, S., and Shukla, A., (1995), "Fiber-optic Acoustic Sensor for Nondestructive Evaluation," *J. of Optics and Lasers in Engineering*, **22**(2), pp. 137-148.

12. Ansari, F., ed., (1993), Applications of fiber optic sensors in engineering mechanics: a collection of state-of-the-art papers in the application of fiber optic technologies to civil structures, American Society of Civil Engineers, New York.

13. Weiss, J.D., (1989), "Fiber-optic strain gauge," *J. Lightwave Tech.*, **7**(9), pp 1308-1318.

14. Vaziri, M., and Chen, C., (1992), "Etched Fibers as Strain Gauges," *J. Lightwave Tech.*, **10**(6), pp.836-841.

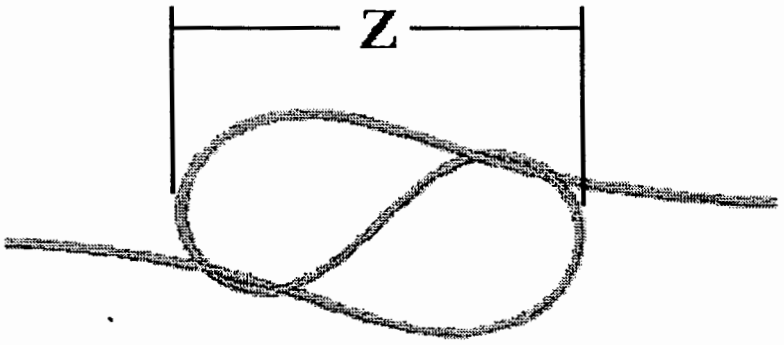

Figure 1. Sketch of the fiber sensor configuration.

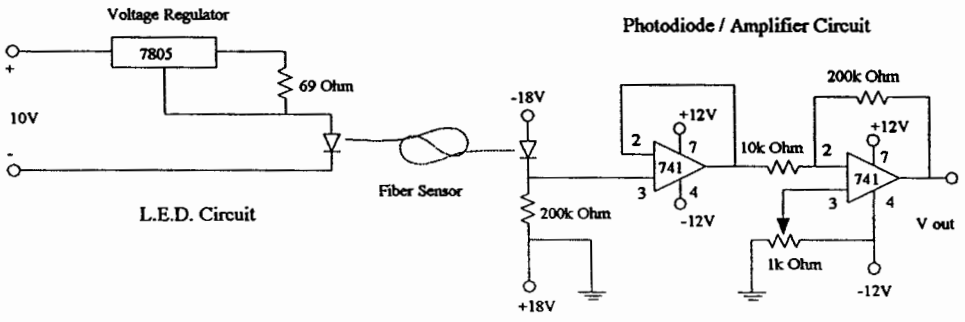

Figure 2. Schematic of the circuit set up for the fiber sensor.

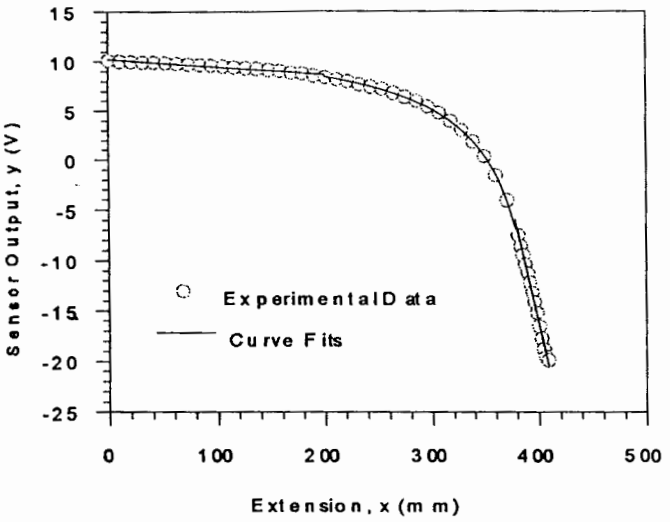

Figure 3. Entire plot of sensor output for a total extension of 410 mm.

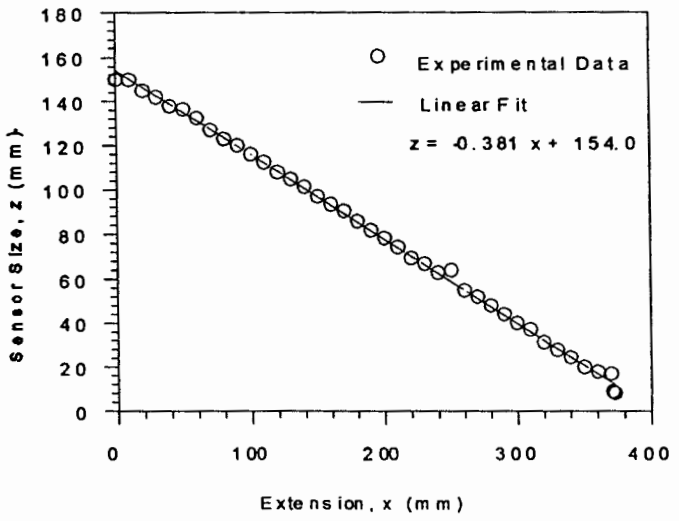

Figure 4. Linear relationship between sensor size and sensor extension.

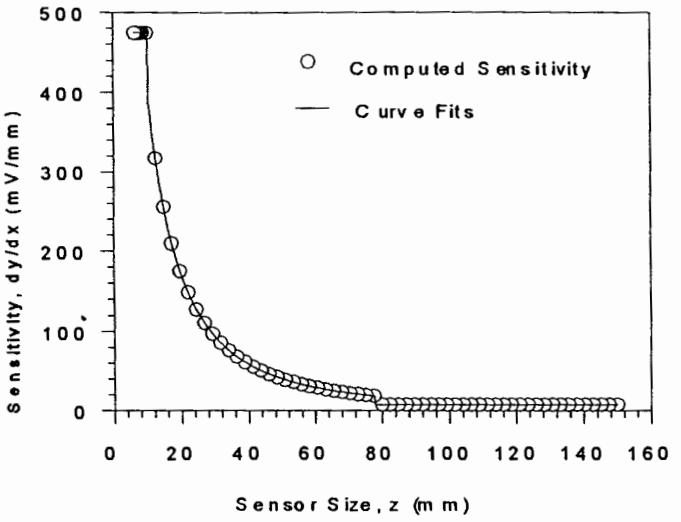

Figure 5. Plot of sensitivity (calibration factor) versus sensor size for the fiber sensor.

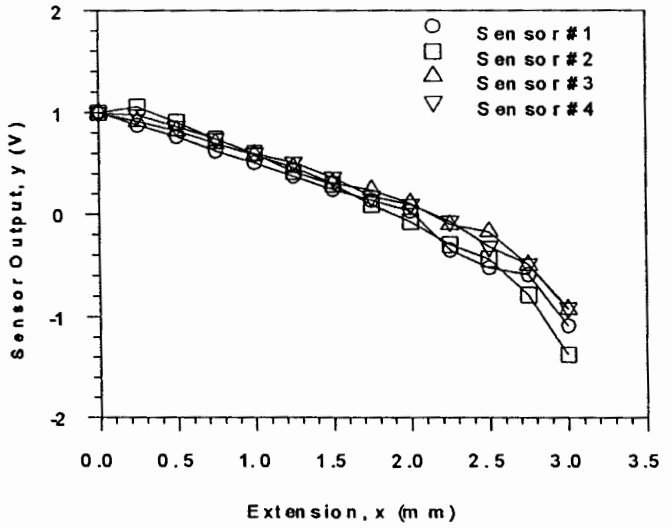

Figure 6. Plot of sensor output versus extension for four different sensors to determine the repeatability of construction.

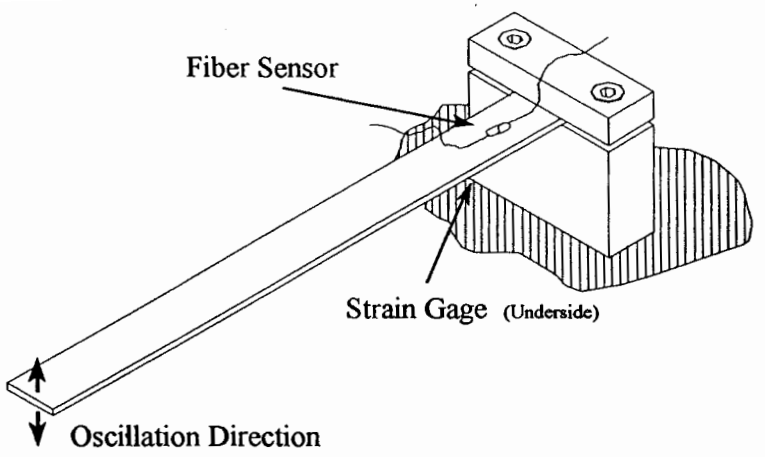

Figure 7. Illustration of a cantilever beam with fiber sensor and strain gage mounted to opposite sides.

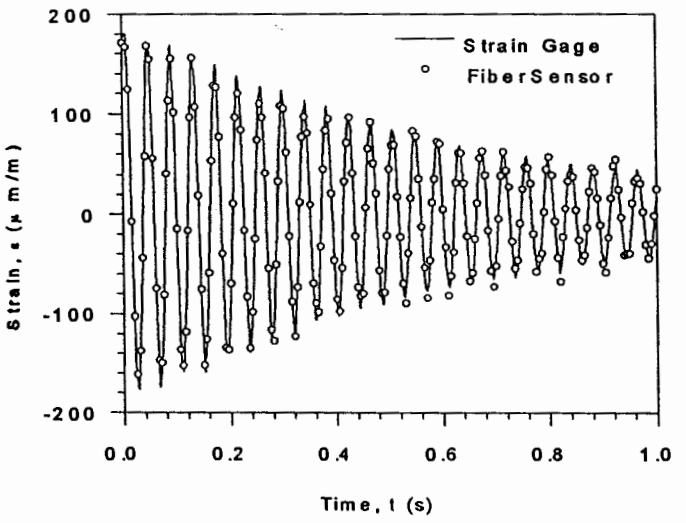

Figure 8. Plot of fiber sensor output and strain gage output for a vibrating cantilever beam (25 Hz).

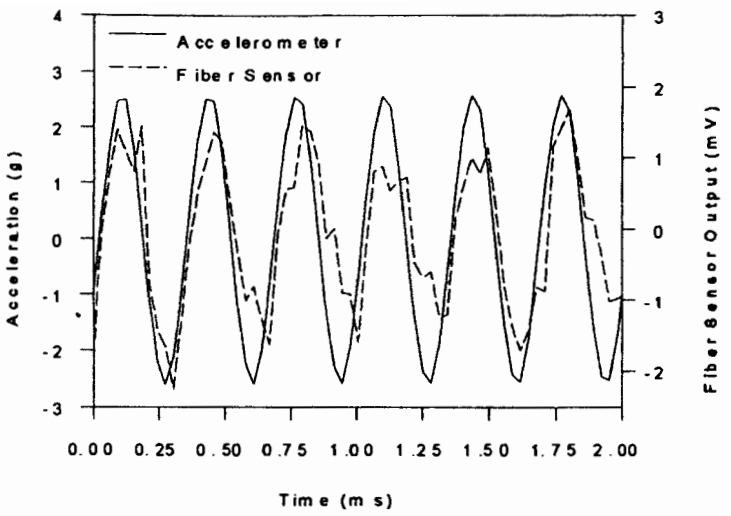

Figure 9. Simple time series comparing the accelerometer output in g's and fiber sensor output in volts.

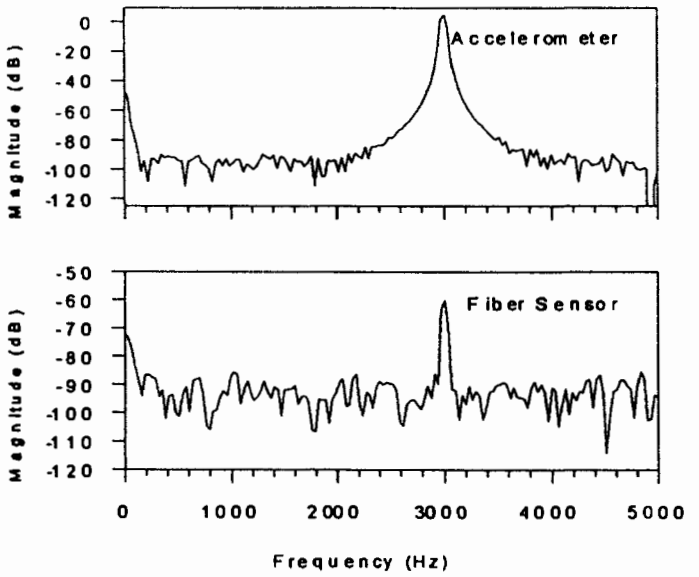

Figure 10. Fast Fourier transform of the data from the 3 kHz experiment showing the good correspondence between the accelerometer and the fiber sensor.

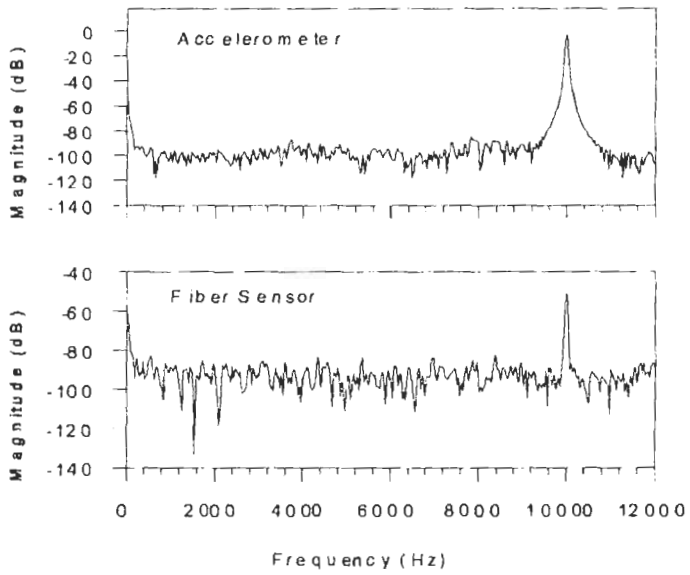

Figure 11. Fast Fourier transform of the 10 kHz data showing that the fiber sensor is still in excellent agreement with the accelerometer.

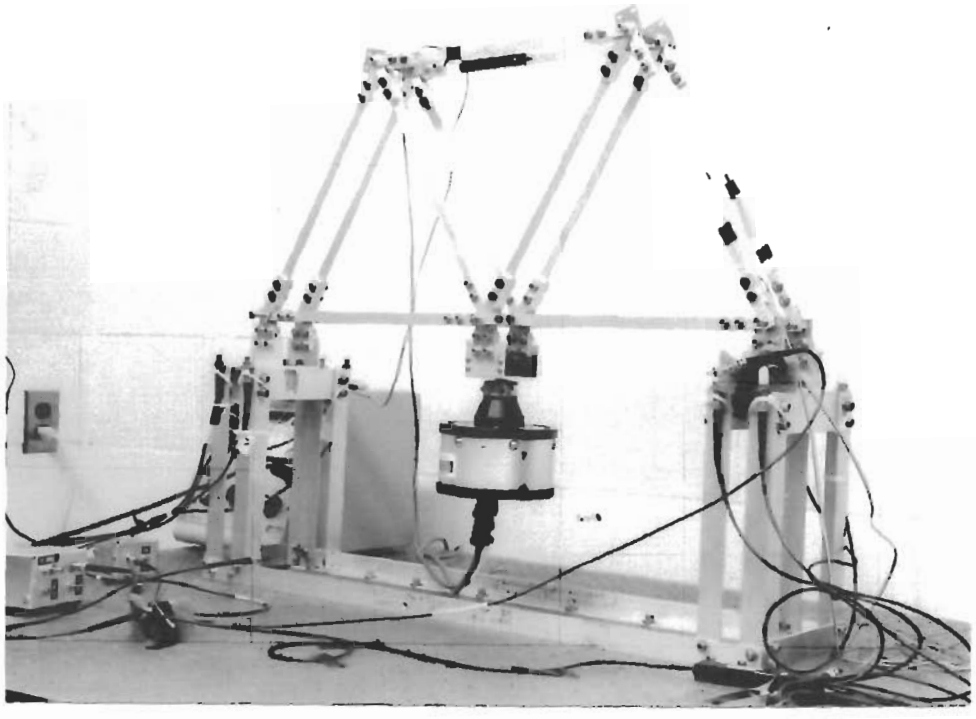

Figure 12. Photograph of the truss type model bridge structure for evaluation of the fiber optic sensor performance.

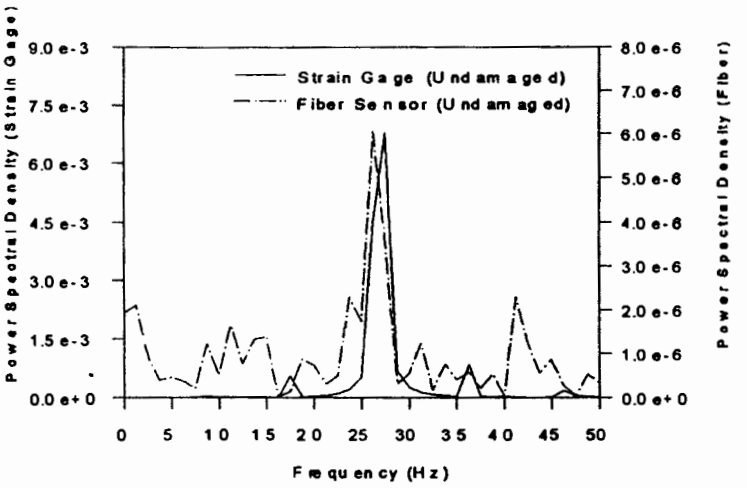

Figure 13Strain gage and fiber sensor response from the bridge structure subject to a dynamic excitation.